UNIVERSITY OF CALIFORNIA,
IRVINE

Quantifying feedbacks between phytoplankton elemental stoichiometry and marine biogeochemistry

DISSERTATION

submitted in partial satisfaction of the requirements
for the degree of

DOCTOR OF PHILOSOPHY

in Earth System Science

by

Nicola A. Wiseman

Dissertation Committee:
Professor J. Keith Moore, Chair
Professor Adam C. Martiny
Professor Francois Primeau

2023

DEDICATION

To

My grandparents

For instilling a love of science within me

And the opportunity to pursue it fearlessly

TABLE OF CONTENTS

LIST OF FIGURES

LIST OF TABLES

ACKNOWLEDGEMENTS

I would like to thank my committee chair, Professor J. Keith Moore.

I would like to thank my committee members, Professor Adam C. Martiny and Professor Francois Primeau.

In addition, I would like to thank my collaborators, Benjamin Twining, Natalie Mahowald, Douglas Hamilton, Rob Letscher, and Patrick Rafter.

Chapter 1 of this dissertation is a reprint of the materials as it appears in Wiseman, N. A., Moore, J. K., Twining, B. S., Hamilton, D. S. & Mahowald, N. M. Acclimation of phytoplankton Fe:C ratios dampens the biogeochemical response to varying atmospheric deposition of soluble iron. *Global Biogeochem. Cycles* (2023), used with permission from the American Geophysical Union. The co-authors listed in this publication are Keith Moore, Benjamin Twining, Douglas Hamilton, and Natalie Mahowald.

Financial support was provided by the University of California, Irvine, the Jenkins family, the division of Ocean Science (OCE) of the Directorate for Geoscience of the National Science Foundation grant OCE-1848576 and the Department of Energy, Biological and Environmental Research Division, Earth System Modeling Program grants DE-SC0016539 and DE-SC0022177.

VITA

Nicola A. Wiseman

2018 B.S. in Environmental Science, University of Rochester

2020 M.S. in Earth System Science, University of California, Irvine

2023 Ph.D. in Earth System Science, University of California, Irvine

FIELD OF STUDY

Marine ecosystem modeling and biogeochemistry in Earth System Models

PUBLICATIONS

Wiseman, NA, Moore, JK, Twining, BS, Hamilton, DS, & Mahowald, NM (2023). Acclimation of phytoplankton Fe:C ratios dampens the biogeochemical response to varying atmospheric deposition of soluble iron. *Global Biogeochemical Cycles*.

Ustick LJ, Larkin AA, Garcia CA, Garcia NS, Brock ML, Lee JA, Wiseman NA, Moore JK, Martiny AC (2021) Metagenomic analysis reveals global-scale patterns of ocean nutrient limitation. *Science*, **372**(6539):287-291.

Weber T, Wiseman NA, Kock A (2019) Global ocean methane emissions dominated by shallow coastal waters. *Nature communications*, **10**(1):4584.

ABSTRACT OF THE DISSERTATION

Quantifying feedbacks between phytoplankton elemental stoichiometry and marine biogeochemistry

by

Nicola A. Wiseman

Doctor of Philosophy in Earth System Science

University of California, Irvine, 2023

Professor J. Keith Moore, Chair

Phytoplankton play a key role in regulating the global carbon cycle by exporting carbon to the deep ocean via the biological pump. The ratio of carbon to nutrients in exported organic matter has long been used to simplify biogeochemical cycles, where a fixed Redfield ratio is assumed. However, these ratios are not truly fixed, and many instances of variation have been observed. Here I aim to illustrate the importance of variable stoichiometry in accurately representing ocean biogeochemical cycling the modern steady state ocean. First, I will highlight the role of variable iron to carbon stoichiometry in coupling of the marine carbon and nitrogen cycles and regulating marine ecosystem response to global changes in atmospheric iron deposition. Second, I will show the impacts of fully variable C:N:P:Fe:Si stoichiometry on biogeochemical cycle interactions and how using a fixed implementation may introduce bias in the interactions between the carbon and nitrogen cycles. Lastly, I will show the roles of individual nutrient variability in driving patterns of nutrient stress and limitation in the modern ocean and how variable stoichiometry plays a role in regulating ocean carbon cycling under nutrient stress.

INTRODUCTION

Carbon dioxide is a potent greenhouse gas that is increasingly emitted to the atmosphere by the combustion of fossil fuels and land use change. The ocean takes up approximately 2.5 $GtCO_2$ yr^{-1}, or roughly 25% of annual global fossil fuel emissions[1]. Ocean biogeochemistry plays a key role in the global carbon cycle through uptake of atmospheric carbon dioxide (CO_2) and long-term storage via the biological and solubility pumps[2]. Phytoplankton help drive the biological pump by taking up dissolved inorganic carbon (DIC) and nutrients and converting them to biomass via photosynthesis. These phytoplankton are then either consumed by larger zooplankton and contribute to carbon cycling within the marine food web or begin to sink and decompose as a component of the sinking particulate organic carbon (POC) flux. As POC sinks, it can be remineralized within the water column, or once exported can be buried, which is a key component of long-term carbon storage.

Earth systems models typically represent phytoplankton in the marine ecosystem by grouping them into phytoplankton functional types, where phytoplankton are grouped by similar traits such as size, grazing relationships, and specific metabolic capacities such as calcification or nitrogen fixation. A small phytoplankton group typically represents pico-eukaryotes, small photosynthetic cyanobacteria such as *Synechococcus* and *Prochlorococcus*, as well as smaller nano-phytoplankton, including calcifiers such as coccolithophores[3]. These phytoplankton contribute highly to primary production due to their efficient nutrient uptake which is attributed to their high surface area to volume ratio. They dominate areas where nutrients are limited such as the Southern Ocean, HNLC regions, and oligotrophic gyres. These small phytoplankton also experience higher grazing pressure than larger phytoplankton. Due to their small size, most phytoplankton (other than coccolithophores) contribute less efficiently to POC export. Coccolithophores, however, form dense ballasts due to their calcium carbonate coccoliths which are efficiently exported[3]. Diatoms are silicifiers that contribute highly to primary productivity under more nutrient replete conditions, such as during spring blooms. They are generally inefficient at nutrient uptake due to their lower surface area to volume ratio. Due to their large size and dense silica frustules, diatoms are efficient carbon exporters. Diatoms contribute to carbon export through direct sinking, aggregation events (often at the end of blooms), and their grazers, which are often large

copepods that form dense, fast sinking fecal pellets. They also have higher nutrient requirements than most small phytoplankton, and therefore respond quickly to nutrient deposition in HNLC regions as long as silica is available[3]. Diazotrophs such as *Trichodesmium* are nitrogen fixers that regulate the ocean reactive nitrogen inventory[3]. They are especially important in nitrogen-limited regions where their N_2-fixing adaptation allows them to supply bioavailable nitrogen to other phytoplankton when remineralized. Diazotrophs are typically iron, phosphorus and/or temperature limited in their growth, and found primarily in mid to low-latitude regions. They have generally lower phosphorus requirements and provide a key link between the nitrogen and phosphorus cycles[4–6]. Phytoplankton help drive the biological pump by taking up dissolved inorganic carbon (DIC) and nutrients and converting them to biomass via photosynthesis.

This organic matter can then be stored in the deep ocean through sinking export, which is then either deposited in ocean sediments or remineralized by bacteria and ultimately returned to the surface by the circulation. The ratio of carbon to nutrients in exported organic matter has long been used to simplify biogeochemical cycles, where a fixed, extended Redfield ratio (C:N:P:Fe) is assumed[7–9]. This ratio helps determine the efficiency of biological export of carbon with respect to limiting nutrients. As marine biogeochemical research has progressed, however, many instances of variation from the traditional Redfield ratio in both sinking organic matter and phytoplankton cells have been observed[10–12]. The environmental drivers of stoichiometric variability have long been a question of interest. One of the simplest mechanisms predicts C:N and C:P for phytoplankton cells as a function of ambient nitrogen and phosphorus concentrations[13]. This simple single-nutrient approach has been supported by a meta-analysis of experimental data, where nutrient availability increases the nutrient:carbon ratio[14]. Using a relatively simple relationship between ambient nutrient supply and nutrient:carbon ratios is incredibly valuable for Earth System Models, which prefer computationally simple relationships to reduce additional computational expenses. While many Earth System Models still implement fixed stoichiometry, some studies have found that utilizing fixed ratios underestimated oceanic CO_2 uptake or resulted in significantly different phytoplankton community compositions under future climate scenarios[9,15–19]. Capturing elemental stoichiometry is key for understanding nutrient

limitation in the surface ocean as well as the strength of the biological pump, a current major source of uncertainty in future climate predictions[20].

Here I aim to further illustrate the importance of including variable stoichiometry in order to accurately represent ocean biogeochemical cycling in the modern steady state ocean and therefore under projected climate change by investigating the roles of variable stoichiometry as a whole and for individual nutrients, and how they interact to regulate the ocean carbon and nitrogen cycles. First, I investigated the impacts of variable Fe:C stoichiometry on the coupling of marine biogeochemical cycles and how the marine ecosystem responds to global changes in atmospheric iron deposition. Second, I studied the biogeochemical impacts of implementing fully variable C:N:P:Fe:Si stoichiometry in a steady state model compared to a fully fixed model to look at how the changes in this parameterization may introduce bias in the interactions between the carbon and nitrogen cycles. Lastly, I investigated the roles of individual nutrient variability in otherwise fully variable and fully fixed models to disentangle the interactions between biogeochemical cycles and the relative roles that individual nutrients and global patterns of nutrient limitation play in regulating ocean carbon cycling in the context of variable phytoplankton elemental stoichiometry.

In my first chapter, I investigate the links between variable phytoplankton Fe:C ratios and marine biogeochemical cycles, using newly available measurements of in situ phytoplankton Fe:C. I found that the observed range of phytoplankton Fe:C variability with increasing ambient dissolved iron concentrations was much greater than the model allowed for and implemented a new range of variability as informed by these measurements. I then ran a series of experiments with various atmospheric iron deposition fields and the improved Fe:C model to investigate the role of dust and pyrogenic sourced iron interactions with phytoplankton Fe:C variability. I ran a series of experiments with pyrogenic Fe only, dust Fe only, dust + pyrogenic Fe, and dust + pyrogenic Fe where the solubility of the pyrogenic iron is doubled to account for uncertainties in pyrogenic Fe solubility. The purpose of these experiments was to look at phytoplankton response to changes in iron deposition that may occur in a changing climate, while also looking at the potential bias that could be introduced in models that do not use a highly variable Fe:C range for phytoplankton.

For my second chapter, I implemented fully variable C:N:P:Fe:Si stoichiometry in order to investigate the role that variable stoichiometry plays in regulating the interactions between biogeochemical cycles. Previously the model had variable P, Fe, and Si quotas, so I introduced a single-nutrient dependency variable N quota, where phytoplankton reduce their N uptake when experiencing nitrogen stress. I used the newly available GO-POPCORNv2 database of particulate organic matter stoichiometry to constrain C:N:P variability within the model[21]. I then compared this new fully variable model to a fixed stoichiometry model to investigate how variable nutrient uptake by phytoplankton allows them to adapt in oligotrophic regions and the downstream effects on the carbon and nitrogen cycles.

For my final chapter, I performed a series of iterative experiments where I fixed/varied individual nutrients in an otherwise variable/fixed run respectively in order to elucidate the role of each nutrient in global biogeochemical cycling, with a particular focus on patterns and drivers of nutrient limitation. I utilized the same variable stoichiometry from the previous study, which is able to reproduce patterns of surface nutrient limitation seen in bottle experiments and metagenomic analysis, to help further explain why carbon export and nitrogen cycling can be so different under fixed versus variable nutrients when global nutrient patterns are relatively similar[22,23]. One goal of this study is to investigate the role of N versus P variability and how these in particular impact modern surface patterns of nutrient limitation. Another goal of this study was to help inform areas of bias that might be introduced by using fixed stoichiometry in models used for future predictions of climate under different emissions pathways.

Overall, the work that I have completed highlights the importance of variable phytoplankton resource acquisition when adapting to different nutrient conditions. My work also shows how observational data from cellular, community, and metagenomic observations can be used to further constrain marine ecosystem representation within earth system models to provide a more realistic representation of biogeochemical cycle interactions under climate perturbations.

CHAPTER 1: Acclimation of phytoplankton Fe:C ratios dampens the biogeochemical response to varying atmospheric deposition of soluble iron

1.1 Introduction

Ocean biogeochemistry plays a key role in the global carbon cycle through uptake of atmospheric carbon dioxide (CO_2) and its long-term storage via the biological and solubility pumps[2]. Phytoplankton help drive the biological pump by taking up dissolved inorganic carbon (DIC) and nutrients and converting them to biomass via photosynthesis. The ratios of carbon to nutrients in exported organic matter have long been used to simplify biogeochemical cycles, where a fixed, extended Redfield ratio (C:N:P:Fe) is assumed[7,8,24]. This ratio helps determine the efficiency of the biological export of carbon with respect to potentially growth-limiting nutrients. Iron is a key micronutrient in this process as it limits phytoplankton growth in regions where other nutrients, such as nitrogen and phosphorus, are readily available[25,26]. These iron limited waters are termed high nutrient, low chlorophyll (HNLC) regions and comprise >33% of the surface ocean[22,23,27]. Nitrogen-fixing diazotrophs are likely to be iron stressed over much of the oligotrophic ocean, linking carbon, nitrogen, and iron cycling in the tropics[5,28,29].

However, a wide range of Fe:C ratios have been observed in both sinking organic matter and *in situ* phytoplankton cells, complicating our understanding of the interactions between iron and carbon biogeochemistry[30,31]. Constraining these nutrient to carbon ratios within models is necessary to properly investigate how ocean carbon cycling will interact with perturbations to nutrient cycling in a changing climate. One expected such perturbation is atmospheric iron deposition, which is sensitive to both climate change and anthropogenic activities, including fossil fuel and biomass burning[32]. Thus, it is important to understand how plankton Fe:C ratios will respond to changing environmental conditions for future projections of ocean biogeochemistry.

Initial measurements of phytoplankton iron quotas relied on either radioisotope uptake experiments or bulk, size fractionation measurements using graphite furnace atomic absorption spectrometry and more recently, inductively-coupled plasma mass spectrometry[33–36]. However, these types of measurements each have some limitations.

Radioisotope uptake experiments derive cellular Fe:C from uptake rates or at steady state, both of which may be impacted by potential bottle effects and rely on the addition of dissolved radiolabeled iron which may lead to ratios that are not representative of the in situ biogenic quotas[31]. Bulk size fractionation analysis via graphite furnace atomic absorption spectrometry and inductively coupled plasma mass spectrometry relies on measurements of the entire size class, which may be skewed by mineral and detrital particles[31]. These methods were also unable to detect low cellular iron concentrations due to detection limits and were unable to provide information on individual taxa versus entire community assemblages[37]. Single-cell synchrotron x-ray fluorescence is a relatively newer method where individual cells are isolated and individually measured for their iron and phosphorus reservoirs, while cellular carbon is estimated from cell volume[24,37].

Fe:C uptake by phytoplankton is primarily controlled by dFe availability in HNLC regions where nitrogen and phosphorus are replete[36]. Measurements of individual taxa iron requirements have found high variation between groups, where coastal species can vary more than 100-fold (2-200) while open ocean species vary by about a factor of 20 (10-200)[38,39]. Some coastal phytoplankton and oceanic diatoms continue to accumulate iron under iron replete conditions -- up to 70 times higher than is needed to reach their maximum growth rate, suggesting that they are capable of luxury storage[36,40,41]. Differences in uptake rates between species were largely attributed to variations in cell surface area, where uptake rate is a function of the surface area to volume ratio and therefore smaller cells are more efficient at iron uptake due to the diffusive limitation of transport[36,42–44]. Smaller prokaryotic cells may also use siderophore-bound iron in order to increase their uptake, potentially leading to higher Fe:C ratios than larger eukaryotes in low-Fe settings, although some species of diatoms have also been found to use iron complexed to siderophores[36,44,45]. Some variation in iron requirements between taxa has also been attributed to the specialized needs of certain groups. For example, nitrogen fixers such as *Trichodesmium* need iron for the nitrogenase enzyme that is required in order to reduce dinitrogen and have been found to contain highly variable iron quotas, with Fe:C ratios ranging from 22-480 µmol Fe/mol C[46–48]. Phytoplankton community composition can strongly influence the strength of the biological pump, as different phytoplankton groups dominate under different conditions and have varying export efficiencies[49,50]. It is therefore important to accurately represent both

the community composition as well as the nutrient requirements of the community to understand ocean carbon cycling.

Nitrogen fixers such as *Trichodesmium* are capable of converting dinitrogen gas (N_2) to a biologically useable form, ammonium (NH_4^+). These marine nitrogen fixers are integral to the marine environment, where other autotrophs are primarily nitrogen limited and represent a significant contribution to the marine nitrogen budget, with rates of nitrogen fixation between 125-223 $TgNyr^{-1}$ [51]. However, the growth of nitrogen fixers is limited by phosphorus and iron availability[4,26]. Therefore, the productivity of these nitrogen-fixers represents a key link between the carbon and nitrogen cycles[28]. The nitrogen and carbon cycles are also linked through fixed nitrogen removal via heterotrophic denitrification and anaerobic ammonium oxidation (anammox). Heterotrophic denitrification is the sequential microbial reduction of nitrate (NO_3^-) to N_2, and anammox is the chemoautotrophic oxidation of ammonium to N_2. Within the water column, these primarily occur where organic particles sink through oxygen minimum zones, with global nitrogen loss rates estimated between 55-73 $TgNyr^{-1}$ [51]. This process connects the rates of particulate matter export to the global nitrogen cycle, as greater export above oxygen minimum zones leads to greater rates of denitrification, and therefore a greater loss of fixed nitrogen from the marine environment. Iron availability limits the growth of diazotrophs and modifies the sinking flux of organic matter into the OMZs. Thus, there are strong links and feedbacks between iron deposition, nitrogen cycling, and the marine carbon cycle[5,28,50,52].

Limited field observations have shown that phytoplankton Fe:C is generally elevated in regions of higher ambient iron concentrations. In the North Atlantic subtropical gyre, under the North African dust plume transport pathway, phytoplankton Fe:C can reach upwards of 90 μmol/mol[24]. Ratios also tend to be higher in coastal regions, where there is a significant continental shelf iron source due to shallower depths. These ratios tend to be lower in more remote regions that have lower atmospheric iron inputs, such as in the Indian subtropical gyre and the Southern Ocean, where ratios tend to be in the 3-15 μmol/mol range[53,54].

Using fixed Redfield values for the C:N and C:P of phytoplankton in ocean models has been found to underestimate carbon fluxes or overestimate nutrient fluxes, especially in oligotrophic, strongly nutrient-limited regions[9,13,15–17,55,56]. About half of the CMIP6 models

account for variable Fe:C ratios while the others assume a fixed stoichiometry[19]. Few studies have investigated the impacts of variable iron stoichiometry in climate scenarios. Buitenhuis and Geider developed an iron-light colimitation model for phytoplankton growth, which allowed for luxury uptake of Fe[57]. This has been implemented in the ocean biogeochemical model PISCES-v2 and allows for phytoplankton iron to carbon ratios up to 40 μmol/mol[58]. Recent work with PISCES found that the linking of the iron and carbon cycles via biological Fe:C is key to controlling nutrient limitation patterns in the future ocean, with direct impacts on net primary productivity, particularly in the equatorial Pacific[59]. Another study using the PISCES model connected the role of diatoms with variable iron quotas to enhanced carbon export in the Southern Ocean and pointed out the necessity of further constraining diatom physiology in this region[60]. Variations in atmospheric iron input strongly impact spatial patterns of phytoplankton growth limitation and the areal extent of the HNLC regions at the global scale[50,52,59]. It may therefore be necessary to include variable iron ratios in ocean models to accurately predict the biogeochemical responses to future climate change.

The primary sources of iron to the oceans are from atmospheric deposition, terrestrial runoff and rivers, continental shelf sediments, and hydrothermal vent systems[61]. In the subtropical and tropical oceans, atmospheric deposition tends to be the primary source of bioavailable iron, while in the polar regions the relative importance of continental shelf and hydrothermal vent dust likely increases[61,62]. Atmospheric iron deposition can represent more than 50% of the iron inputs to the euphotic zone in many regions[52]. This atmospheric iron deposition is composed of two primary components: desert mineral dust and pyrogenic aerosols[32,63]. The FeMIP model intercomparison project reported atmospheric iron deposition over a very wide range of 1.4-32.7 Gmol Fe yr^{-1} imposed in current ocean models, reflecting large uncertainties in this key ocean forcing[64].

Only a fraction of the iron in the dust and pyrogenic aerosols is soluble upon deposition to the oceans. The solubility percentage of iron within desert mineral dust is highly uncertain, with estimates ranging from 1% to as high as 12%, with ocean biogeochemical models having previously often assumed a constant 1-2% solubility of the iron from dust sources[30,65–70]. Conversely, iron from pyrogenic sourced aerosols may be more soluble, and despite making up a smaller fraction of the total deposition, could potentially represent a significant portion of soluble iron deposition in many regions[32,71–73].

Recent atmospheric iron model intercomparison studies have shown that including this pyrogenic sourced iron is key to simulating observations of variations in iron solubility over the global ocean and that iron from pyrogenic wildfire sources stimulates the biological pump at a greater rate than iron from mineral dust[32,71,74,75]. However, there are large uncertainties in constraining these pyrogenic sources in terms of their sources, solubilities, and fluxes, and previous estimates of pyrogenic sourced iron may be significantly underestimated[76–79].

Here we seek to address several key questions regarding the links and feedbacks between variable phytoplankton Fe:C ratios and marine biogeochemical cycling. What is the relationship between phytoplankton Fe:C ratios and ambient dFe concentrations? What are the impacts of variable phytoplankton Fe:C ratios on marine biogeochemical cycling? We compare model implementations with fixed, weakly varying, and strongly varying Fe:C ratios, evaluating against observational datasets. We also examine how incorporation of dynamic Fe:C ratios influences the marine biogeochemical response to variations in atmospheric deposition of soluble iron. We combined estimated depositions of pyrogenic and dust sourced iron in different ways to provide a wide range in soluble iron inputs from the atmosphere (1.5 - 7.0 Gmol Fe/yr). Generating the deposition estimates in this manner also allowed for some assessment of the relative biogeochemical impacts of the pyrogenic and dust sourced iron.

1.2 Methods

We use the Community Earth System Model (CESM) ocean circulation, marine ecosystem and biogeochemistry components. The version used is modified from CESM v1.21 but includes most science modifications that were introduced in CESM v2.0, including variable phytoplankton phosphorus quotas and an explicit ligand, iron model[51,80]. The model contains three explicit phytoplankton groups: diatoms, nano- to pico-sized phytoplankton (a fraction of which is assigned an implicit calcifier group) and diazotrophs[26,80]. The rate of nitrogen fixation by diazotrophs is proportional to their carbon fixation, where the amount fixed is the demand left after their uptake of nitrate and ammonium is calculated. The rate of denitrification is proportional to the amount of particulate organic carbon and dissolved organic carbon being remineralized in low oxygen conditions. When oxygen concentration

is <5 μM, nitrate is consumed rather than oxygen during the remineralization of this organic matter[5]. The model has one class of explicit, iron-binding ligands and external iron sources from atmospheric deposition (pyrogenic and mineral dust sourced iron), marine sediments, hydrothermal vents, and riverine inputs[5,80]. We ran the simulations with constant pre-industrial CO_2 for 300 years and averaged the results over the last 20 years of the simulation.

The iron uptake rate and the Fe:C for new growth of these groups are a function of ambient iron concentration and a prescribed half-saturation constant but vary only within a narrow range (2.5-6 μmol/mol for small phytoplankton and diatoms, and 14-48 μmol Fe/mol C for the diazotrophs[26]. Here we test a much wider range of Fe:C ratios. The cellular iron to carbon ratio for new growth (gQfe) is assumed to be a linear function of the ambient dissolved iron concentration[36]. FeOpt is the group-specific, dissolved iron concentration where the Fe:C reaches its maximum value; above this concentration, the Fe:C for new growth is set at the prescribed maximum value (gQfe_max). When dissolved iron concentrations fall below FeOpt, the Fe:C for new growth decreases linearly with iron concentration proportional to FeOpt until the prescribed minimum value is reached (gQfe_min), which is imposed at lower dFe concentrations:

$$\mathrm{gQfe} = \min\left(\mathrm{gQfe\_max}, \max\left(\mathrm{gQfe\_min}, \mathrm{gQfe\_max} \cdot \frac{\mathrm{dFe}}{\mathrm{FeOpt}}\right)\right) \qquad \text{Eq. 1.1}$$

where gQfe is the Fe:C ratio for new growth, gQfe_max is the prescribed maximum Fe:C, gQfe_min is the prescribed minimum Fe:C, dFe is the local concentration of dissolved iron, and FeOpt is the iron concentration where Fe:C reaches its maximum value (Fig. 1.1). The iron concentration where the minimum is reached is therefore dependent on the prescribed FeOpt, gQfe_max, and gQfe_min values, and can be calculated by the following:

$$\mathrm{dFe\_min} = \mathrm{FeOpt} \cdot \frac{\mathrm{gQfe\_min}}{\mathrm{gQfe\_max}} \qquad \text{Eq. 1.2}$$

$$\mathrm{VFe} = \frac{\mathrm{dFe}}{\mathrm{dFe} + \mathrm{kFe}} \qquad \text{Eq. 1.3}$$

Phytoplankton growth rate is calculated according to Liebig's law of the minimum, where the relative uptake rate for each nutrient (Eq. 1.3, N, P, Fe, Si, ranging from 0-1) is calculated, and the lowest value determines the relative growth rate, after which temperature and light are also considered multiplicatively. Phytoplankton growth limitation due to iron is therefore dependent on the ambient iron concentration and the iron half-saturation constant

for each plankton group. We assume a fixed, minimal value for the zooplankton Fe:C of 3.0 µmol Fe/mol C, with excess ingested iron routed to dissolved iron via excretion. The Fe:C ratio of the phytoplankton is passed to the sinking export generated by aggregation and grazing. Zooplankton mortality provides additional export with low endmember Fe:C. Thus, the Fe:C ratio in the sinking biogenic export has an Fe:C value typically lower than the phytoplankton at that location. However, if scavenged iron is included, the sinking Fe:C is always higher than the phytoplankton Fe:C.

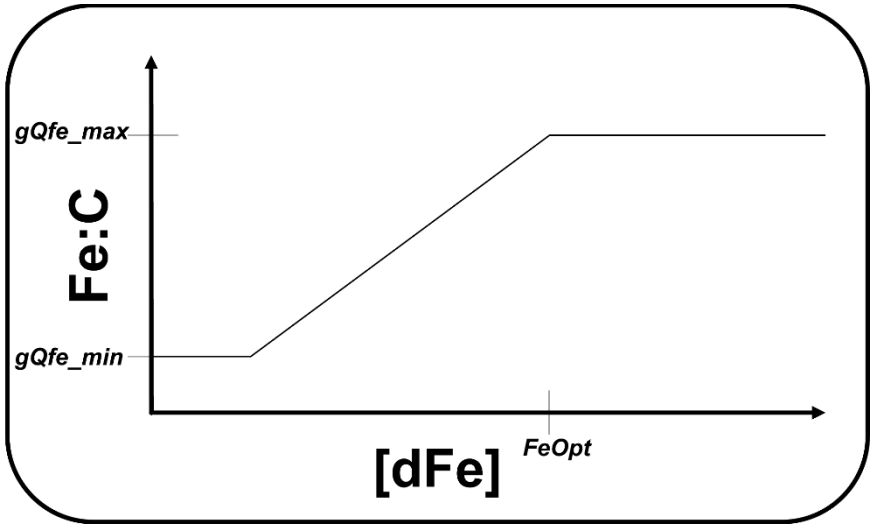

Figure 1.1. Phytoplankton Fe:C ratio for new growth as a function of dissolved iron. FeOpt determines the dissolved ambient iron concentration at which phytoplankton Fe:C reaches its maximum value (gQFe_max). Fe:C varies linearly with dissolved iron concentration between the prescribed, group-specific maximum (gQFe_max) and minimum (gQfe_min) quotas.

We test applying a broader range of Fe:C ratios, specific for each phytoplankton group, based on our compiled database of field observations (Table S1.1 in supplemental materials (SM) for more details) of phytoplankton Fe:C where ambient dissolved iron was also measured (n = 142), including unpublished Arctic data from the Twining lab[24,31,35,41,44,48,53,54,81–87]. These observations include bulk Fe:C as well as individual phytoplankton Fe:C for small phytoplankton, diatoms, and nitrogen fixers (Table S1.1). Based on these observations, we test a range of maximum Fe:C ratios for new growth (gQFe_max) from 6.0 to 120 µmol Fe/mol C (12 - 240 µmol Fe/mol C for diazotrophs,

intervals of 10 μmol Fe/mol C) as well as a range of FeOpt values from 1.25 nM to 2.0 nM (1.25 nM, 1.4 nM, 1.6 nM, 1.75 nM, 2.0 nM specifically) for each phytoplankton group. We use an optimal maximum gQFe_max of 90 μmol Fe/mol (180 μmol Fe/mol for diazotrophs) and an FeOpt of 1.75nM for all phytoplankton groups based on this tuning, where we aimed to best represent the observations of phytoplankton Fe quotas. Varying these parameters had little to no impact on globally integrated NPP or POC Export, varying between 52.6-52.7 PgC/yr and 8.36-8.46 PgC/yr, respectively. We also compare to observed global distributions of nutrients including iron, nitrogen, and phosphorus, where nitrogen and phosphorus are from World Ocean Atlas[88]. Observational iron data is largely from the GEOTRACES project, supplemented with historical data compilations[62,89,90].

In order to investigate the impacts of variable plankton Fe:C stoichiometry on the coupling of the iron and carbon cycles, we compare simulations with the optimized variable Fe quota model with simulations using fixed Fe:C values of 3.0, 7.0, and 10.0 μmol Fe/mol C. We also compare variable versus fixed quotas in response to different levels of atmospheric iron deposition. We conducted a series of experiments with four different atmospheric iron deposition fields: pyrogenic Fe only, dust Fe only, dust + pyrogenic Fe, and dust Fe + pyrogenic Fe deposition where the solubility of the pyrogenic iron is doubled to account for uncertainties in the pyrogenic solubility[32]. The dust deposition was extracted from the CMIP6 CESM2 historical simulation, averaged over the years 1990-2009[80]. We assume the mineral dust is 3.5% iron by weight and apply a spatially varying solubility for the aerosol iron at deposition. The ratio of coarse/fine dust at deposition is a useful proxy for the distance traveled from the mineral dust source regions, as the coarse dust particles are expected to be removed more quickly during atmospheric transport. The dust iron solubility in CESM2 is a function of the ratio of coarser dust particle deposition / finer dust particle deposition[80]. The approach gives low solubilities near dust sources (~0.5%) increasing to greater than 10% in the most remote regions in the central Pacific, capturing the observed relationship between deposition rate and iron solubility seen in observations[91]. Here, we use a recently optimized version of the relation between the dust deposition large/small ratio and solubility. The deposition of iron from pyrogenic sources used includes soluble iron from wildfires and anthropogenic emissions with month-to-month seasonality[50], here scaled up from 1.37 to 1.5 Gmol Fe yr^{-1}. The deposition assumes a constant solubility in pyrogenic

aerosols of 5%, which is in the lower range of previous estimates. We include a scenario where pyrogenic aerosols have a constant solubility of 10%, which is closer to estimates from the CAM6 model, where wildfire sourced iron has a solubility of 18.8% and anthropogenic iron has a solubility of 11.2%[32,50]. CESM2 currently simulates pyrogenic iron in a simpler manner, relating pyrogenic iron deposition to black carbon deposition in the model[80].

We force the ocean model with the pyrogenic soluble iron deposition combined with the soluble iron deposition from mineral dust in our optimal case. We include sensitivity experiments where we force the ocean model with only the pyrogenic-sourced iron and with only the dust-sourced iron. The global rate of soluble iron deposition for the pyrogenic and dust sources to the surface ocean is 1.5 Gmol Fe yr^{-1} and 4.0 Gmol Fe yr^{-1}, respectively, resulting in a total global deposition of 5.5 Gmol Fe yr^{-1}. A fourth sensitivity experiment combines the dust iron with the pyrogenic-sourced iron globally scaled by a factor of two (total 7.0 Gmol Fe yr^{-1}), to account for uncertainties in the solubility and aerosol source strengths, which may be greater than the initial pyrogenic-sourced iron estimate (Fig. 1.2). One goal is to evaluate the importance of the pyrogenic iron source in driving marine biogeochemistry. These experiments provide a wide range of estimates of the atmospheric deposition of soluble iron to the oceans (1.5 - 7.0 Gmol Fe yr^{-1}). Each experiment was performed with the optimal, variable Fe:C stoichiometry range of 3-90 μmol Fe /mol C (6-180 μmol Fe/mol C for the diazotrophs) as well as with a fixed Fe:C stoichiometry at value of 7 μmol Fe /mol C, for comparison.

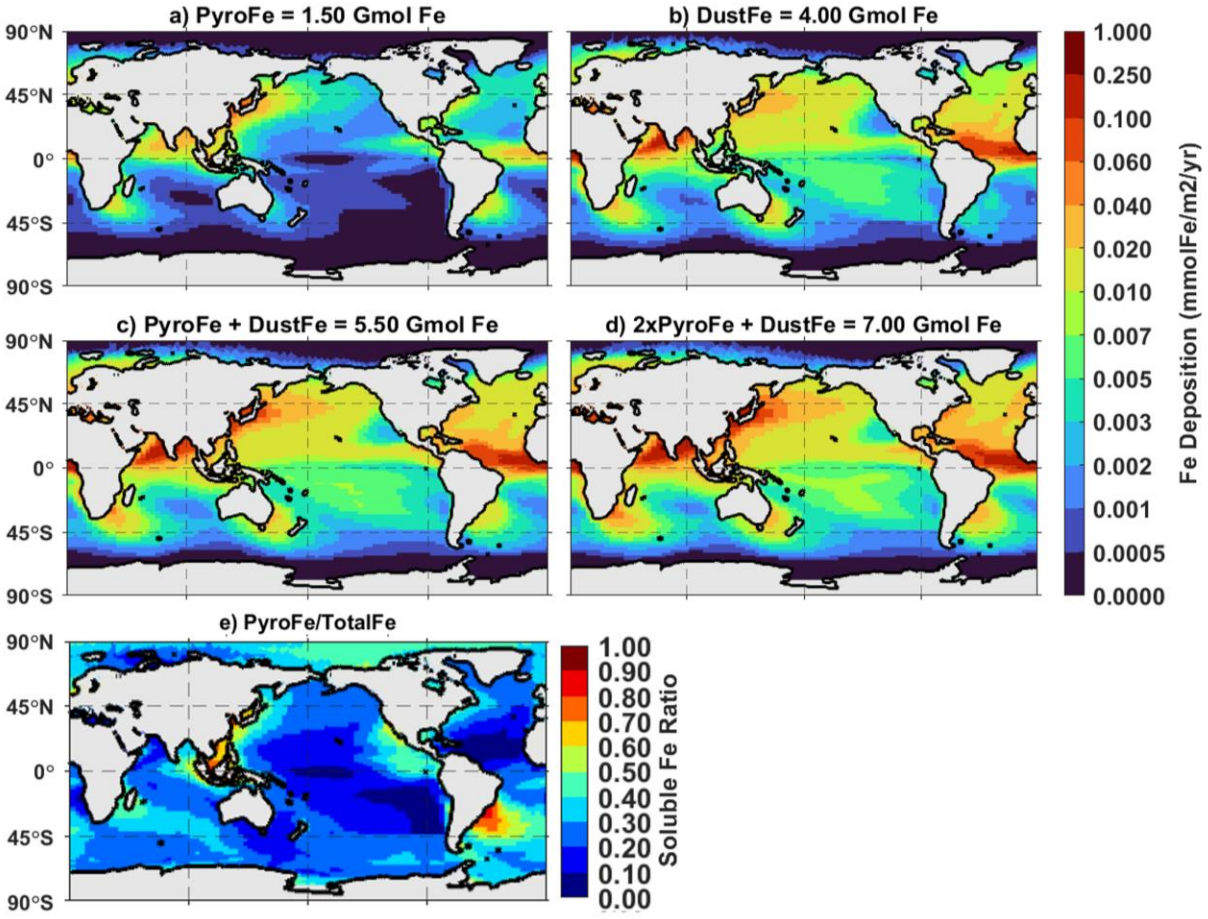

Figure 1.2. Atmospheric soluble iron deposition fields used to force the ocean biogeochemistry model. (a) PyroFe includes soluble iron from wildfires and anthropogenic combustion for an annual ocean surface deposition of 1.50 Gmol Fe (Hamilton, Moore et al., 2020). (b) DustFe includes soluble iron from lithogenic sources for an annual ocean surface deposition of 4.00 Gmol Fe. (c) Annual ocean surface soluble iron deposition from pyrogenic and lithogenic sources totaling 5.50 Gmol Fe. (d) Annual ocean surface soluble iron deposition from pyrogenic and lithogenic sources where the pyrogenic solubility is doubled for a total deposition of 7.00 Gmol Fe. (e) Ratio of pyrogenic sourced iron deposition from wildfires and anthropogenic combustion divided by total soluble iron deposition from pyrogenic sources and mineral dust.

Note that the pyrogenic soluble iron deposition exceeds the dust iron inputs considerably in the eastern and western North Pacific and in the western South Atlantic and

exceeds 10% of the total soluble iron deposition everywhere but the North Atlantic subtropical gyre and the most remote Pacific regions (Fig 1.2e).

1.3 Results

We find that a broad Fe:C range for new growth (3-90 μmol Fe/mol C for the small phytoplankton and diatoms and a range of 6-180 μmol Fe/mol C for diazotrophs) best reproduces the patterns in field observations of phytoplankton Fe:C versus surface iron concentration, increasing the overall skill of the model (Fig. 1.3). CESM previously had varying Fe:C within a limited range of 2.5-6 μmol Fe/mol C for diatoms and small phytoplankton and 14-48 μmol/mol for diazotrophs[26]. Each group has an optimal dFe concentration for growth of 1.75 nM, so the maximum iron quotas are achieved only in the highest dFe surface concentration regions. The tuned model with these parameters is able to reproduce the observed relationship between phytoplankton Fe:C and in situ dFe, where dissolved iron concentrations increase, so do the observed Fe:C ratios (Fig. 1.3a,). In the field observations, cellular Fe:C increases roughly linearly with dissolved iron variability with both axes on a $\log_{10}$ scale (Fig. 1.3a). The observed range of Fe:C ratios for small phytoplankton was 3-100 μmol Fe/mol C and for diatoms was 4-528 μmol Fe/mol C[31,54]. The variable iron quota model better captures the observed relationship between Fe:C and ambient iron concentrations (Spearman's correlation r_s of Fe:C vs dFe from observations, the tuned model, and the previous limited-range model were 0.45, 0.87, and 0.83, respectively, Fig. 1.3a). The model Fe:C also generally agrees with the individual cell iron to carbon measurements (Fig. 1.3b). For each individual cell measurement, we extracted model Fe:C for the same phytoplankton group at the same location. The optimized variable model better captures these individual cell Fe:C measurements compared to the limited range model and fixed model with a Fe:C ratio of 5 μmol Fe/mol C (Fig. S1.1). Using the expanded variable range did not degrade the model performance matching observations of surface nitrate, phosphate, and iron (Table S1.2). When compared to World Ocean Atlas 2018, the r_s for surface nitrate (5m depth) decreased from 0.916 to 0.909 and the RMSE decreased from 2.41 μM to 2.29 μM. The r_s for surface phosphate (5m depth) increased from 0.924 to 0.928, comparing the limited-range and variable models, while the root mean squared error

(RMSE) decreased from 0.188 µM to 0.181 µM. For iron, the r_s increased from 0.445 to 0.490 and the RMSE decreased from 1.288 nM to 1.265 nM. .

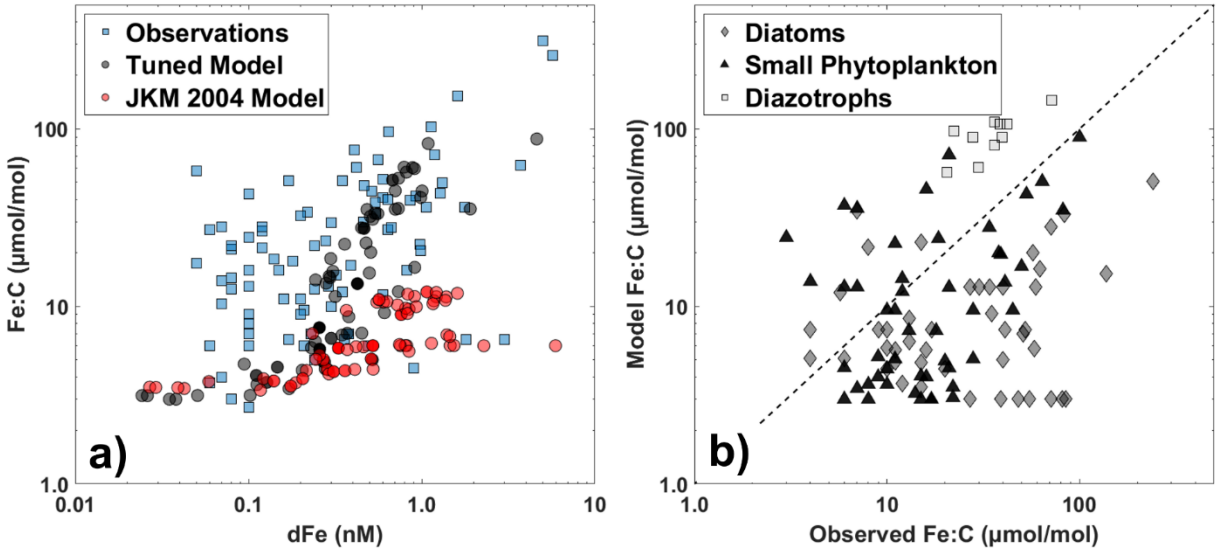

Figure 1.3. Comparison of field observations and simulated Fe:C of phytoplankton and ambient dFe concentrations (a) and phytoplankton Fe:C in observations and simulations (b). Observed community Fe:C as a function of dFe (a, blue squares), tuned model Fe:C versus dFe (a, gray circles), previous model Fe:C versus dFe (a, red circles) extracted from the same locations as the field observation. Observations Spearman's correlation $r_s = 0.45$, $p << 0.05$ (1e-5), tuned model $r_s = 0.87$, $p << 0.05$ (5e-27), previous model $r_s = 0.83$, $p << 0.05$ (1e-22). (b) Phytoplankton group specific model Fe:C versus observed phytoplankton Fe:C (gray diamonds are diatoms $r_s = 0.13$, black triangles are small phytoplankton $r_s = 0.28$, white squares are diazotroph $r_s = 0.63$). Model estimates were paired based on location and phytoplankton type. Dashed black line in (b) represents a 1:1 fit.

Overall, the model is able to reproduce the observed spatial variations between the Atlantic, Pacific, and Southern Oceans (Fig. 1.4). Phytoplankton Fe:C is elevated in regions where surface dFe is elevated due to regional inputs such as high atmospheric dust deposition, coastal shelf sources, and upwelling. Diazotroph Fe:C measurements are limited to the North Atlantic while some small phytoplankton and diatom measurements are available for most ocean basins. However, even within a small region the model is able to

replicate the gradient of decreasing Fe:C ratios for the diazotrophs, as dFe decreases from near coast to more offshore (Fig. 1.4).

Regions where the model and observations diverge may be driven by colimitation. For example, the model underestimates diatom Fe:C in the oligotrophic southern Pacific gyre, where the observed values seem very high compared with other regions. Twining et al. (2021) suggested nitrogen limitation may lead to increases in the cellular Fe:C ratios, as the nitrogen limitation would decrease the frequency of cell division, allowing for iron to accumulate within diatom cells as luxury iron uptake[41]. This is not seen in the small phytoplankton community because they are expected to maintain their growth rates even in low-nutrient regions due to their higher surface to volume ratios, and because they have much less capacity for luxury uptake and storage. Our model does not allow for luxury uptake, but rather sets the uptake proportional to current growth requirements. The r_s values for model Fe:C for each group versus the observations (small phytoplankton, diatom, diazotrophs) were 0.28, 0.13, and 0.63 respectively for the variable quota model, while they were 0.13, 0.23, and 0.17 respectively, with the original limited-range model.

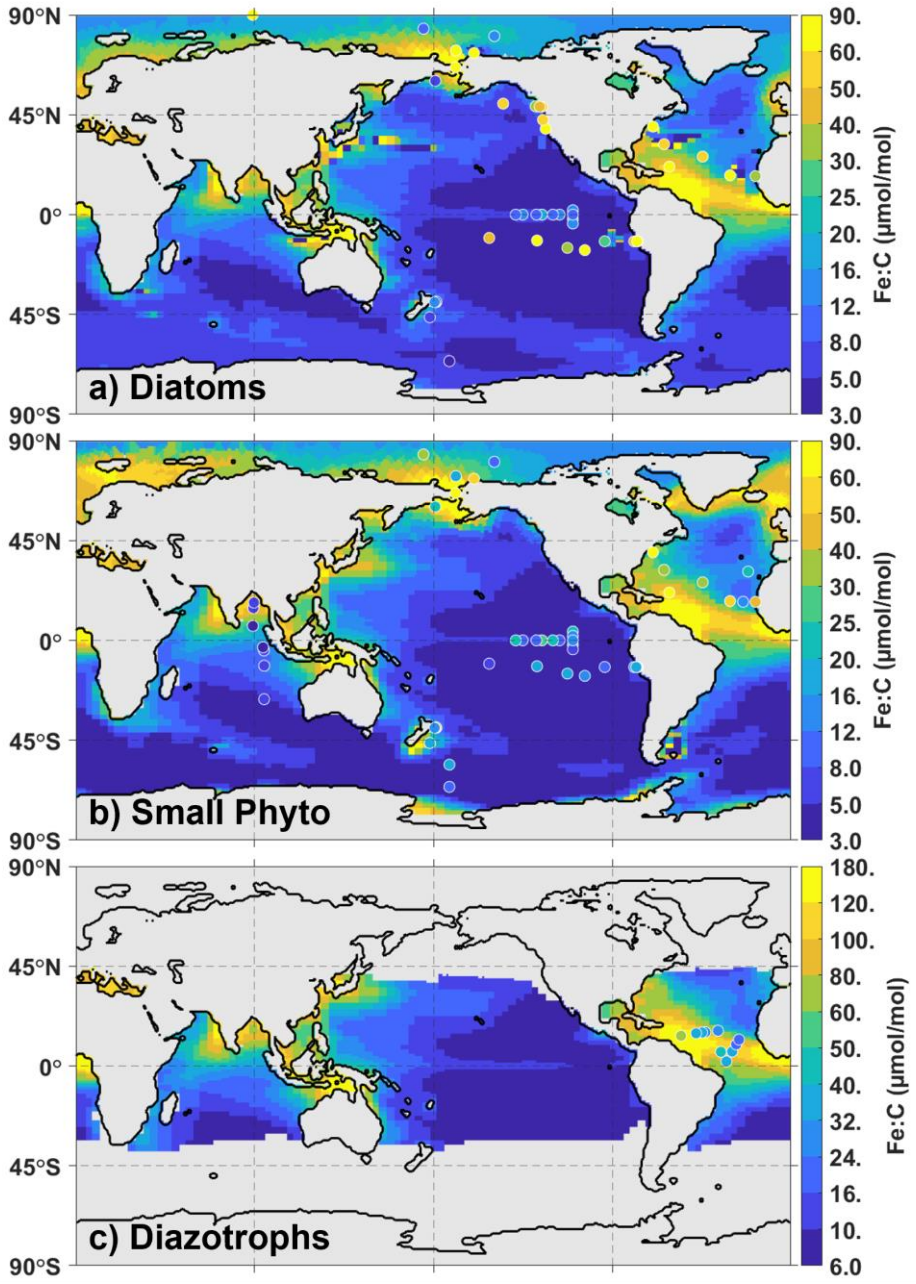

Figure 1.4. Optimized model patterns of (a) diatom group Fe:C overlaid with circles showing observations of diatom Fe:C (r_s = 0.13), (b) small phytoplankton group Fe:C overlaid with circles showing observations of small phytoplankton Fe:C (r_s = 0.28), and (c) diazotroph group Fe:C overlaid with circles showing observations of diazotroph Fe:C (r_s = 0.63).

1.3.1 Fixed vs Variable Fe Quotas

We find that using fixed stoichiometry in place of variable stoichiometry has first order impacts on nutrient cycling within the surface ocean. One method to quantify this impact is the HNLC index. We define an HNLC region in the Pacific Ocean between 25°N and 25°S, east of 150°E, and the HNLC index as the area in the HNLC region that has surface nitrate concentrations greater than 0.3 µM in the model output, divided by the same metric for nitrate from the World Ocean Atlas 2018 (WOA18)[88]. With the expanded variable Fe:C range, we are able to reproduce the HNLC size as seen in the WOA18, with an HNLC index of 1.0063 (Fig. 1.5). With fixed stoichiometry, the HNLC extent can be captured with a fixed Fe:C of 5 µmol/mol but expands or retracts rapidly with other fixed stoichiometries. For fixed Fe:C ratios of 3, 5, 7, and 10, the HNLC areal extent changes by -54%, -2%, +44%, and +81%, respectively (Fig. 1.5).

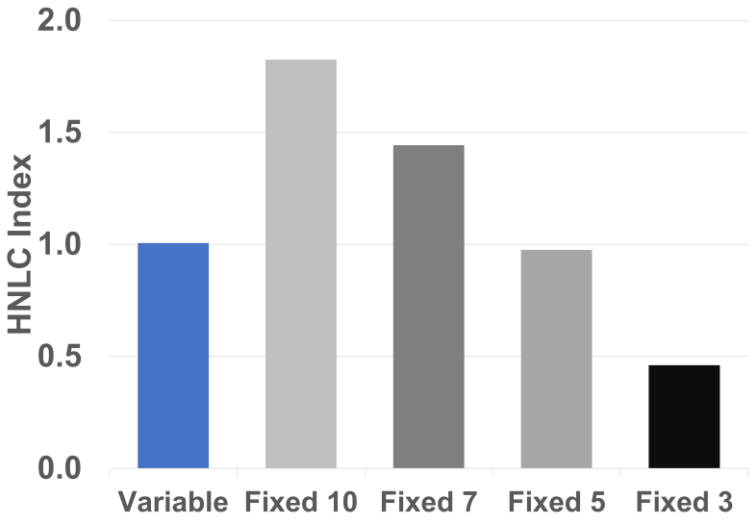

Figure 1.5. HNLC index for five simulations within the Central Pacific HNLC region (between 25°N and 25°S, east of 150°E). Index is defined as the ratio of ocean surface area where nitrate concentrations exceed 0.3 µM in each simulation compared to the WOA18. Variable is the tuned model with variable Fe:C ranging from 3-90 µmol Fe/mol C for small phytoplankton and diatoms and 6-180 µmol Fe/mol C for diazotrophs, the fixed scenarios of 10, 7, 5, and 3 are where the model phytoplankton Fe:C is fixed for all groups at 10, 7, 5, and 3 µmol Fe/mol C, respectively.

Comparing the fixed ratio models versus the optimized variable Fe quota model, there are modest impacts on carbon fluxes (NPP, export) integrated at the global or Central Pacific HNLC region scales (Table 1.1). However, there are large shifts in the spatial patterns of NPP and carbon export across the simulations, with disproportionate impacts on key fluxes within the marine nitrogen cycle. Global NPP decreased by up to 5% with fixed quotas, and NPP in the HNLC region decreased by up to 9% (Table 1.1). The regional NPP response to the chosen fixed value for Fe:C is non-linear, with the fixed value of 7 μmol Fe/mol C having the weakest response of a 3% decrease, while the 3 and 10 μmol Fe/mol C versions had stronger decreases of 7% and 9%. The 3 and 10 Fe:C cases have more biased Fe/C ratios relative to the observations, leading to strong regional over/underestimates of productivity and export, which influence downstream regions. The variations in HNLC size are not strongly dependent on the specific values of gQFe_max and FeOpt (Fig. S1.2).

The optimized variable model, limited-range model, and fixed ratio of 5 μmol Fe/mol C, all generally reproduce observed variations in dissolved iron concentrations for the top 100m (Fig. S1.3). However, the limited variable model and the 5 μmol Fe/mol C have larger positive biases in the Saharan dust plume. In the North Atlantic from 0° to 20°N (iron bias 0.226 nM for the variable model, 0.6578 nM for the limited-range, and 0.703 nM for fixed stoichiometry). Low, fixed Fe:C values will lead to positive iron biases in high dust regions because the biological export will be underestimated. This would lead to overestimation of the lateral export of iron away from the high input regions.

Table 1.1. Changes in key annual global and regional carbon fluxes in the optimal model when fixed stoichiometry is used versus the expanded variable range. Percentages are percent change from the tuned variable model where Fe:C ranges from 3-90 μmol Fe/mol C for small phytoplankton and diatoms and 6-180 μmol Fe/mol C for diazotrophs. The fixed scenarios of 10, 7, 5, and 3 are where the model phytoplankton Fe:C is fixed for all groups at 10, 7, 5, and 3 μmol Fe/mol C, respectively. NPP is net primary productivity, POC is particulate organic carbon, HNLC is Central Pacific high nutrient low chlorophyll region between 25°N and 25°S, east of 150°E.

Fe:C	NPP (PgC/yr)	POC Export (PgC/yr)	Nitrogen Fixation (TgN/yr)	Water Column Denitrification (TgN/yr)	HNLC NPP (PgC/yr)	HNLC POC Export (PgC/yr)
Variable	53.8	8.5	225.3	63.1	13.6	2.03
Fixed 10	51.2 (-5%)	8.0 (-6%)	173.1 (-23%)	20.6 (-67%)	12.4 (-9%)	1.74 (-14%)
Fixed 7	52.8 (-2%)	8.3 (-2%)	201.6 (-10%)	40.6 (-35%)	13.2 (-3%)	1.93 (-5%)
Fixed 5	53.5 (-1%)	8.5 (0%)	228.4 (+1%)	67.2 (+7%)	13.5 (-2%)	2.02 (-2%)
Fixed 3	53.3 (-1%)	8.6 (+2%)	260.6 (+15%)	102.4 (+62%)	12.7 (-7%)	1.94 (-4%)

Surface chlorophyll spatial patterns shift sharply in the tropical Pacific in response to the treatment of plankton Fe quotas (Fig. 1.6). While the optimized model is able to reproduce patterns seen in satellite chlorophyll products (log-transformed r = 0.60). A fixed ratio of 10 μmol Fe/mol C results in up to 60% underestimation of surface chlorophyll in the equatorial upwelling zone, while the more western region of the Pacific sees overestimates of up to 60%. This is most likely due to the excess nitrogen and phosphorus not utilized in the equatorial upwelling region due to the high iron requirements being transported laterally to the oligotrophic gyres increasing chlorophyll concentrations from less than 0.05 mgChl/m^3 to between 0.05 and 0.10 mgChl/m^3. In contrast, using a fixed Fe:C ratio of 3 μmol Fe/mol C results in an overestimate of chlorophyll in the equatorial upwelling tongue by

greater than 100%. This is due to the increase in iron availability from the lack of efficient iron export, leading to a buildup of available iron in the surface waters. This allows for phytoplankton to increase their biomass to a greater extent than they would under stronger iron limitation, thereby driving the increase in surface chlorophyll. However, due to the reduced iron limitation, the surrounding areas transition to nitrogen limitation, resulting in a decrease in surface chlorophyll outside of the equatorial upwelling tongue. The fixed ratio of 5 μmol Fe/mol C was able to reproduce a chlorophyll pattern and HNLC extent similar to the variable model, however there is much greater chlorophyll in the coastal region of the equatorial upwelling region due to the rigidity of the Fe:C ratio, similar to the 3 μmol Fe/mol C case, although to a milder extent. The variable Fe quota model, which gives high Fe:C in the plankton near the coast and very low Fe:C values in the offshore waters, is best able to replicate the satellite chlorophyll patterns. Fixed ratio models cannot match this high iron to low iron transition in the Fe:C ratio, leading to regional dissolved iron biases, as noted above for the North Atlantic.

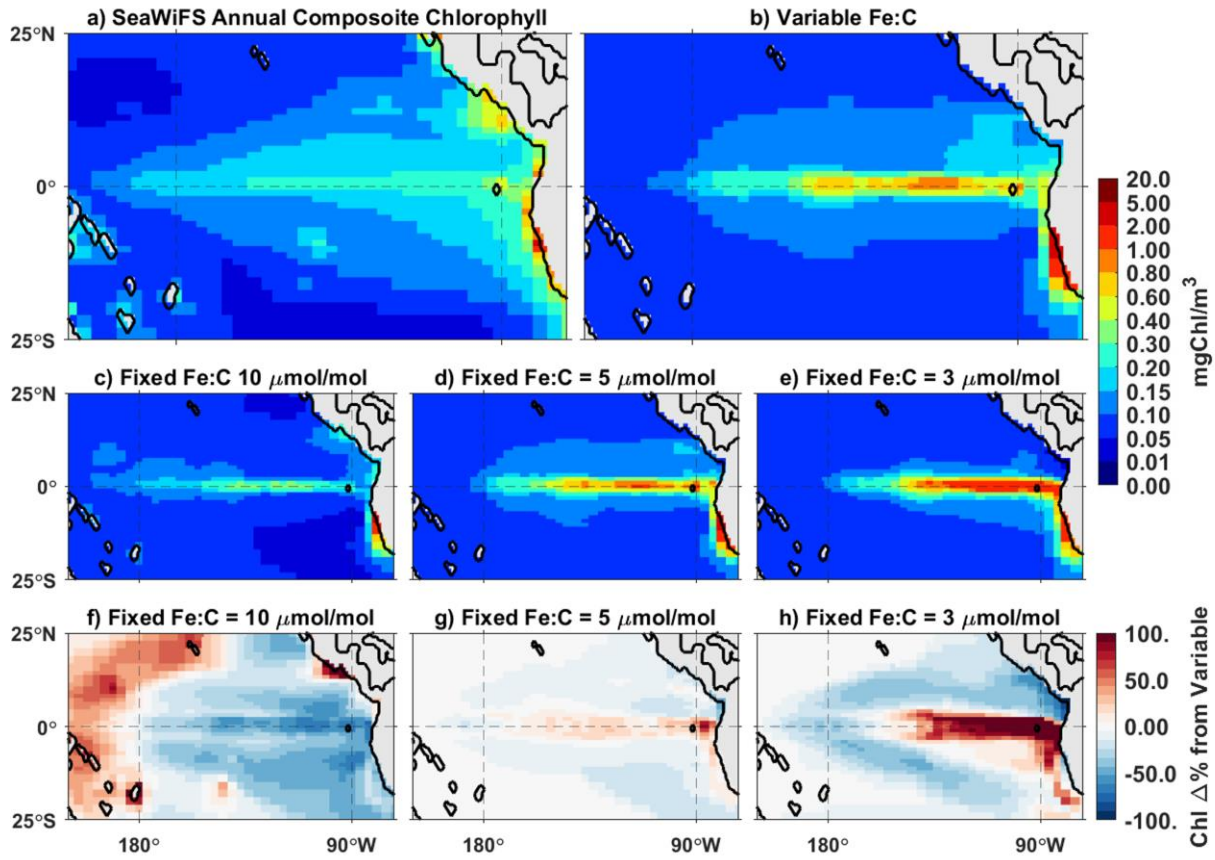

Figure 1.6. SeaWiFS chlorophyll climatology (a) and optimized model surface chlorophyll (b, mgChl/m^3) for our HNLC region. Middle panels show surface chlorophyll for fixed Fe:C simulations (c-e), bottom panels show the percent change of chlorophyll for fixed Fe:C simulations (f-h) compared to the dynamic iron quota model.

There are also large shifts in the spatial patterns of sinking particulate organic carbon (POC) export in this region (Fig. 1.7). The simulation with a fixed Fe:C of 5 µmol Fe/mol C had the pattern most similar to the variable quota model. In the 10 µmol Fe/mol C simulation most of the sediment-sourced iron is used up nearshore, with little advection to the open ocean (Fig. 1.7c). In contrast, with the 3 µmol Fe/mol C quota, much less iron is used up nearshore, and there is a much larger lateral flux of iron to the open ocean. These shifts in the spatial patterns of export influence the amount of organic matter sinking into the oxygen minimum zones, leading to large swings In the rates of water column denitrification, even though the integrated POC export changes only modestly at the global or regional scale (Table 1.1).

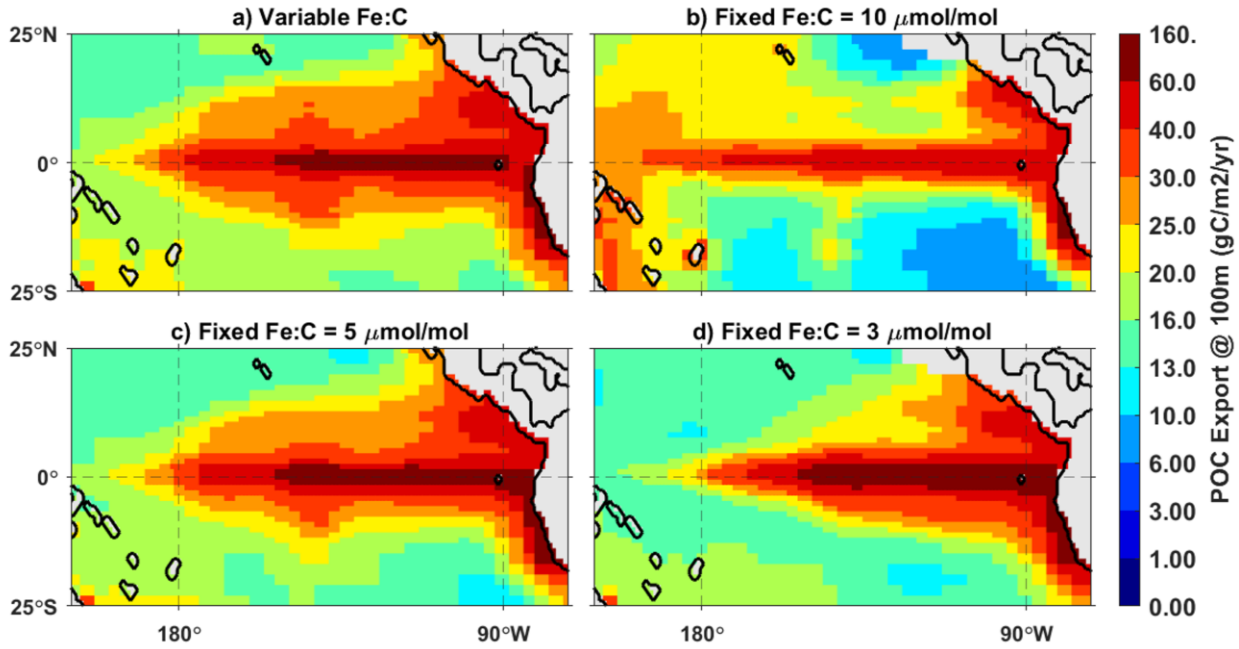

Figure 1.7. Sinking particulate organic carbon (POC) export at 100m depth comparing the dynamic Fe:C model (a) and with simulations using fixed Fe:C ratios of 3, 7, and 10 μmol Fe/mol C (b-d, respectively).

Varying plankton iron quotas change the efficiency of the biological export of iron. This can have strong impacts on the spatial patterns of nutrient limitation as iron becomes exported more or less efficiently relative to the other nutrients. With a fixed Fe:C ratio of 10 μmol Fe/mol C, the iron-limited areas expand substantially, compared with the variable Fe:C simulation (Fig. 1.8). The iron-limited area for the small phytoplankton group increases from 37.4% of total ocean area with variable Fe:C, up to 38.9% and 56.78% with the fixed Fe:C of 5 and 10 μmol Fe/mol C respectively (Fig. 1.8). This is because iron is already limiting in the HNLC regions, and when higher Fe:C ratios are prescribed, iron is exported more efficiently per unit carbon, resulting in even less iron being available and therefore stronger iron limitation. With a fixed ratio of 3 μmol Fe/mol C, the HNLC region outside of the equatorial upwelling zone transitions from iron limitation to nitrogen limitation, as less iron is exported per mol of carbon and iron limitation is weakened. This results in the regional transition to nitrogen limitation, as nitrate supply can be readily consumed when iron is available.

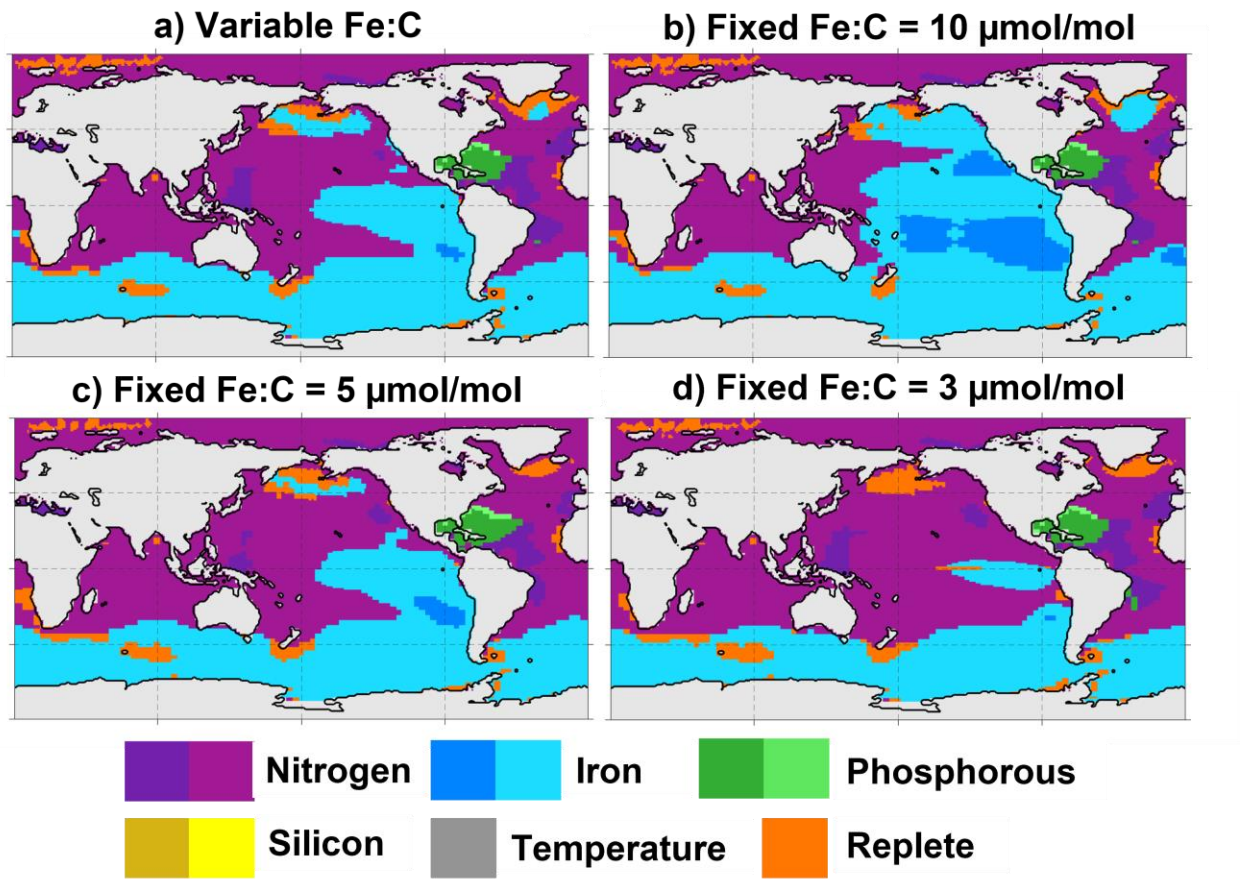

Figure 1.8. Patterns of nutrient limitation of small phytoplankton growth from variable and fixed iron quota simulations. Phytoplankton are nutrient replete when nutrient limitation reduces growth by less than 10%. Darker color shading indicates where growth is reduced by more than 50% from the maximum growth rate. The tuned model is shown in (a) and the simulations using fixed Fe:C ratios of 3, 5, and 10 µmol Fe/mol C (b-d) respectively.

1.3.2 Impacts of Varying Iron Deposition on Ocean Biogeochemistry

We compare simulations with variable and fixed Fe:C stoichiometry across a range of atmospheric deposition rates (1.5-7.0) Using variable stoichiometry dampens the impacts of changing iron deposition on the global ocean carbon cycle compared with fixed Fe:C (Table S1.2). At lower deposition rates, using fixed Fe:C has a larger impact on carbon cycling, with NPP 15% lower and sinking particulate organic carbon (POC) 51% lower when a fixed Fe:C of 10 µmol Fe/mol C is used versus the variable ratios (Table 1.2).

With increasing deposition, NPP and sinking POC do not respond as strongly when using variable versus fixed stoichiometry, with NPP and POC being 0.4% lower and 1% higher respectively (Table 1.1). There is a modest change in NPP from low deposition to high deposition (50.3-53.8 PgC/yr) when the optimal variable Fe:C is used. By having dynamic, variable iron quotas, phytoplankton are able to partially dampen, or buffer, the effects of changing iron deposition by decreasing Fe:C when iron is scarce to maintain productivity. Increasing Fe:C ratios lead to more efficient export of iron with increasing iron deposition. Thus, models with fixed Fe quotas will overestimate the biogeochemical impacts of varying iron deposition, by not accounting for this phytoplankton acclimation to available nutrient concentrations.

Table 1.2. Percent change in key carbon fluxes for the pyrogenic iron scenarios compared to the optimal deposition scenario with variable stoichiometry in the equatorial HNLC area and globally.

Deposition	**Fe:C**	**Global NPP**	**Global POC Export**	**HNLC NPP**	**HNLC POC Export**
CESM2opt 5.5 Gmol Fe/yr	Variable	53.8 PgC	8.5 PgC	13.6 PgC	2.03 PgC
PyroFe	Variable	-7%	-9%	-15%	-21%
1.5 Gmol Fe/yr	Fixed 7	-13%	-14%	-32%	-37%
DustFe	Variable	+0.2%	-1%	+2%	+0.3%
4.0 Gmol Fe/yr	Fixed 7	-3%	-4%	-4%	-8%
DustFe + 2xPyroFe	Variable	-0.4%	+1%	-2%	-1%
7.0 Gmol Fe/yr	Fixed 7	-2%	-1%	-3%	-4%

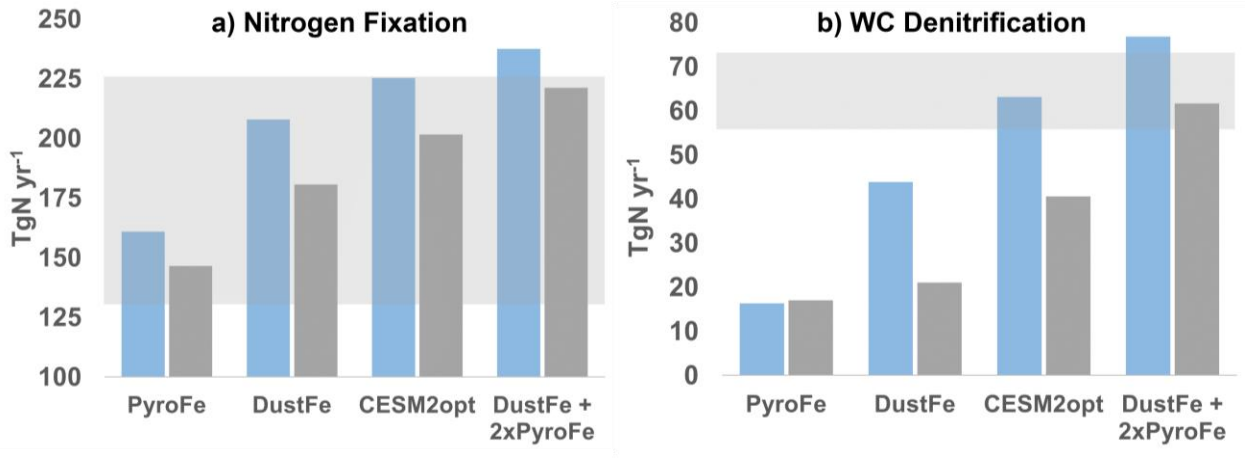

Figure 1.9. Global annual nitrogen fixation (a) and water column denitrification (b) under the various iron deposition scenarios for the optimized variable model (blue) and fixed Fe:C of 7 µmol Fe/mol C scenarios (dark grey). The gray boxes represent the estimated ranges for nitrogen fixation and water column denitrification from a recent inverse model study (Wang et al., 2019).

The variations in atmospheric iron inputs have strong impacts on global nitrogen fluxes in conjunction with the fixed or optimized variable Fe quota models. When atmospheric deposition is decreased (PyroFe and DustFe simulations), both nitrogen fixation and water column denitrification decrease drastically. The reduction in nitrogen fixation can be attributed to the decrease in diazotroph productivity. Diazotrophs are iron limited in much of the surface ocean. Therefore, when the atmospheric deposition is decreased, their productivity is reduced, and global rates of nitrogen fixation decrease accordingly. The decrease in water column denitrification can be attributed to a general decrease in productivity and carbon export, especially in the eastern Pacific where iron is the primary limiting nutrient. This impacts the HNLC regions in particular, which increase in area by 23% when pyrogenic sourced iron is omitted, and iron limitation expands to regions that were previously nitrogen limited (Figure S1.4). With the reduction of atmospheric iron deposition and stronger iron limitation, primary productivity decreases, resulting in less organic matter sinking through the oxygen deficient zones. With less organic matter to degrade, water column denitrification drops dramatically. This feedback between iron limitation and water column denitrification is one of the key links between the iron and

nitrogen cycles. Proper estimates of iron deposition are necessary in order to accurately simulate the global marine nitrogen cycle. When the optimal iron deposition field is used, the simulated global nitrogen fixation rate is 225 TgN yr^{-1}, while the global water column denitrification rate is 63 TgN yr^{-1}, which are both in agreement with recent inverse model estimates[51] (Fig. 1.9).

1.4 Conclusions

Phytoplankton Fe:C uptake links not only the oceanic iron and carbon cycles, but strongly impacts the marine nitrogen cycle as well. It is therefore important that the representation of phytoplankton iron quotas in biogeochemical models reflect the observed biological patterns. This requires not only variable quotas, but also a large variable range to best represent the flexibility of these phytoplankton groups under a changing environment. We find that a range of 3-90 μmol Fe/mol C for the small phytoplankton and diatoms and a range of 6-180 μmol Fe/mol C for diazotrophs better represents the spatial variability of individual cell iron to carbon ratios between ocean basins as well as the observed relationship between iron to carbon and dissolved iron concentrations.

Our results suggest that using a nutrient-dependent "frugal phytoplankton" approach to stoichiometry can capture some of the observed variation in phytoplankton iron to carbon ratios[13]. The expanded range is also in agreement with previous studies, such as Person et al., (2018), where expanded diatom Fe:C variability in the lower range resulted in improved model representations of surface chlorophyll in the Southern Ocean[60]. There is considerable uncertainty in the parameter values for the maximum and minimum Fe quotas. The phytoplankton Fe:C observations provide a way to tune these parameters so ocean models can capture the observed spatial variations in Fe quotas. We expect that the exact values of the model parameters could differ across models due to differences in other factors, such as the scavenging parameterizations and the levels of external iron inputs. The HNLC index was relatively insensitive to FeOpt values between ~1-2 nM (Figure S1.2). Fixed Fe:C ratio models will generate larger regional biases in surface iron concentrations and less accurate spatial patterns of nutrient limitation. Additional in situ observations are needed to better constrain these parameter values, in terms of determining the iron concentration where the community begins to acclimate to increasing iron stress by modifying their quotas.

Using the increased iron stoichiometry variability does not significantly impact the surface nutrient patterns yet leads to diverging responses to changes in soluble iron deposition. This highlights the utility of biological information such as observations of phytoplankton Fe:C ratios to informing prognostic models. While the surface nutrient fields that are typically used to tune the model parameters are not significantly impacted, we can instead use the novel information provided by the individual phytoplankton cell measurements to constrain their Fe:C ratios for growth. This approach could prove useful for other parameters within the model, as this biological information can reduce the degrees of freedom present when tuning marine ecosystem models by informing the ranges for parameters that are otherwise determined via guess and check.

The link between iron and carbon via phytoplankton Fe:C uptake has first order impacts on global nutrient cycling. When Fe:C ratios are fixed, surface nutrient distributions are impacted, particularly in regions where atmospheric iron deposition rates are low, i.e., the Pacific HNLC region, leading to changes in the primary limiting nutrient as macronutrients are drawn down or increased. This response is sensitive to the fixed value chosen, and results in significant increases or decreases in the areal extent of these regions (Fig. 1.8). This leads to downstream effects on water column denitrification, as reductions in the POC export to the nearby oxygen minimum zones are reduced when the iron supply is not able to maintain phytoplankton growth (Table 1.1). The study by Person et al., (2018) focused on the ability for diatoms to maintain significant growth rates in low iron conditions, our study reaches a similar conclusion, albeit through a separate mechanism[60]. By allowing phytoplankton iron uptake to be reduced in low iron waters via the Fe:C ratios, there is more iron left available to sustain growth, where a fixed Fe:C may overestimate the iron limitation and the growth rate reduction.

The flexibility of phytoplankton variable iron quotas is key to them maintaining productivity in regions of low deposition as previously mentioned, but also when that deposition changes. When only dust sourced iron is used to force the model, global NPP and POC export are reduced by 3% and 4% respectively when fixed stoichiometry is used. However, when variable stoichiometry is used, NPP and POC export increase by 0.2% and decrease by 1% respectively, showing that phytoplankton are able to acclimate to changes in atmospheric deposition rates. However, this only dampens the biogeochemical response

and there are limits to this acclimation as shown by the reductions in NPP and POC export when only pyrogenic sourced iron is used in both the variable and fixed scenarios, as well as the generally large impacts on nitrogen fluxes (Table S1.2).

Future changes in atmospheric iron deposition under different climate scenarios are still highly uncertain as they will be modified by climate change and anthropogenic activities[50,63,69]. Pyrogenic iron inputs can rival dust sources in some regions. Our results suggest that pyrogenic iron may exceed dust iron inputs in the western North Pacific and western South Atlantic (Fig. 1.2e). We see some of the greatest impacts on carbon and nitrogen cycling under different deposition scenarios in the equatorial Pacific, where export production can directly impact denitrification rates in the OMZs and nitrogen fixation rates in the gyres. In order to make reliable projections of the interactions between marine ecosystems and the cycling of Fe, C, and N, it seems important to include the pyrogenic iron sources, which are significant in magnitude and highly variable through time. Not accounting for this source could result in underestimates of global ocean nitrogen fixation and water column denitrification, which are integral to the global ocean fixed nitrogen inventory, and therefore carbon cycling in a primarily nitrogen-limited ocean[28,50]. Large shifts in the pyrogenic-sourced aerosols are likely in the future, responding to changes in wildfire activity and anthropogenic combustion patterns[69,77,92].

We used observations of phytoplankton Fe:C ratios to constrain the modeling effort. There is a great need for additional field measurements of phytoplankton elemental stoichiometry, but also stoichiometry for other ecosystem components, including within zooplankton and the sinking particulate flux, if we are to unravel the multiple processes modifying the phytoplankton stoichiometry before and after export of organic matter from the euphotic zone. The GEOTRACES program has greatly expanded the global-scale observational datasets for iron and other trace elements[93]. But there are still large uncertainties regarding the marine iron cycle, including the magnitude of different sources, the rates and dynamics of removal by particle scavenging, and in the cycling of the iron-binding ligands. Additional field and laboratory studies are necessary to reduce these uncertainties, and better constrain different aspects of the complex Earth System Models used for climate projection. A better understanding of the biological links between the elemental cycles is critical for understanding current patterns, but also for projecting future

changes in response to climate warming and other anthropogenic activities in the future[28,79,94].

CHAPTER 2: Phytoplankton variable stoichiometry modifies key biogeochemical fluxes and the functioning of the biological pump

Introduction

The biological pump plays a key role in the global carbon cycle, driving ocean uptake and storage of atmospheric carbon dioxide (CO_2)[2]. Phytoplankton are key drivers of the biological uptake of carbon by taking up dissolved inorganic carbon (DIC) and nutrients and converting them to biomass via photosynthesis. Some of this fixed carbon is exported to the ocean interior, lowering surface carbon concentrations. The efficiency of carbon export by the biological pump is a function of the flux leaving the surface ocean, the depth at which organic carbon is respired, and how long the carbon remains at depth, before being transported back to the surface via overturning circulation[79,95,96]. These processes are all sensitive to climate change, but the direction and magnitude of the sensitivity is poorly understood. For example, increases in sea surface temperatures lead to increased stratification in the surface ocean, which can reduce nutrient supply and therefore reduce phytoplankton productivity, but warming also potentially increases the rates of metabolic processes including phytoplankton growth[94,97,98]. There are many compounding interactions associated with these processes that are tied to changes in temperature and nutrient availability, and the global impacts of these changes on the biological pump on longer timescales are poorly constrained, but important to understand for longer-term climate projections[20]. Ocean uptake of atmospheric CO_2 will strongly impact climate evolution on multi-century timescales[79,94].

Phytoplankton growth is primarily limited by nutrient availability. A fixed ratio of carbon to nutrients in the exported organic matter has long been used to simplify biogeochemical cycles, where a fixed, extended Redfield ratio was used to link the cycling of carbon and key growth-limiting nutrients, including nitrogen, phosphorus, iron, and silicon (C:N:P:Fe:Si). However, it is now widely accepted that phytoplankton are capable of variable resource acquisition and that the elemental ratios are not fixed, modulating the efficacy of the biological export of carbon with respect to limiting nutrients[7,8,10,12,44]. Field measurements of particulate matter organic matter stoichiometry find that C:N and C:P

ratios tend to be elevated in the oligotrophic gyres where nutrients are low[99]. C:P ratios can vary by more than a factor of two, where the lowest values are typically observed in the Southern Ocean, which are significantly below Redfield C:P (<80 mol/mol), while the highest values tend to be found in the western North Atlantic and are in excess of 200 mol/mol[99]. C:N variability is much smaller, with its lowest values around 5 mol/mol in the Southern Ocean, and greatest values in the southern Indian Ocean, exceeding 8 mol/mol[99].

An early implementation of variable C:N ratios in particulate organic matter in a steady state ocean model found that using a fixed Redfield C:N underestimated the total dissolved inorganic carbon inventory and ocean pCO_2 uptake, while using the same variable parameterization in a prognostic climate scenario yielded greater anthropogenic CO_2 uptake[9]. A more recent study with variable C:N:P stoichiometry found that a fixed stoichiometry model underestimated the total 21st century ocean carbon uptake by only 0.5 - 3.5%, but that picophytoplankton stock did not decline as greatly as other phytoplankton types due to their greater stoichiometric flexibility, highlighting the importance of variable stoichiometry for predicting changes in marine biodiversity[15]. Other studies utilizing variable phytoplankton C:N:P ratios found that including dynamical ocean biology reduces the sensitivity of biogeochemical cycling to changes in ocean physics[16,17]. This result was supported by a study by Kwon et al., where CMIP6 models that included flexible C:N:P:Fe ratios showed relative increases in net primary productivity (NPP) in future climate simulations compared to fixed ratio models which showed relative decreases[18]. Another study focused on iron cycling in the Pacific found strong links between iron limitation and net primary productivity and highlighted the uncertainty that Fe:C stoichiometry plays in this response[59]. These studies highlight the necessity of variable stoichiometry for properly simulating the interactions between biogeochemical cycles in both steady state and future climate simulations.

We want to further elucidate the interactions between phytoplankton stoichiometry and global ocean biogeochemistry to further understand the role of variable phytoplankton nutrient acquisition in driving patterns of net primary productivity and carbon export. We want to know what the overall impact of variable stoichiometry is on marine biogeochemical

fluxes. We previously showed an important impact from variable Fe:C ratios on carbon export and the spatial extent of the High Nutrient, Low Chlorophyll region in the equatorial Pacific[20]. We hypothesize that fixed stoichiometry will decrease productivity and export in many regions, as phytoplankton will not be able to acclimate to low nutrient availability by reducing their cellular quotas. However, using fixed nutrient:carbon ratios also means that less nutrient will be exported per unit carbon in areas with high nutrient supply, potentially increasing lateral nutrient transport to adjacent regions. Thus, there are downstream effects and complex nutrient interactions, leading to uncertainty about the global, net effects of varying stoichiometry. Earth system models are valuable tools for investigating the interactions between physics, biology, and biogeochemical cycles as they explicitly track individual nutrients, multiple phytoplankton functional types, and realistic ocean physics.

The Community Earth System Model (CESM) module includes an ocean ecosystem and biogeochemistry model that contains three explicit phytoplankton groups (diatoms, pico-nanophytoplankton, a fraction of which acts as an implicit calcifier group, and diazotrophs) with variable nutrient quotas for phosphorus, iron, and silicon[26,51]. The model was recently updated to include greater variability in the phytoplankton iron quotas, with an improved match to observations[100]. Here, we have integrated a new variable nitrogen quota parameterization for phytoplankton, allowing for dynamic computation of phytoplankton C:N:P:Fe:Si ratios as phytoplankton acclimate to changing ambient nutrient concentrations. For each nutrient, the cellular quota (nutrient:C ratio) for new growth is a function of ambient nutrient concentrations, with progressive reductions in the cellular quotas at low ambient nutrient concentrations (Methods, Fig, S2.1).

We find that with the newly implemented variable nitrogen quotas, the model is able to replicate the observed spatial patterns in particulate organic matter stoichiometry. For C:N:P stoichiometry, we compare the model particulate flux at 100m to the surface POM from the GO-POPCORN database for each observational location where the model grid cell is determined using a least squares calculation[101]. An important note is that the observational data is bulk POM and contains heterotrophic bacteria and non-sinking detritus that are not simulated in our model. Our model well represents the relationships between nutrient to

carbon ratios and ambient nutrient concentrations (Fig. 2.1, Fig. S2.2). There is high variability in the observations of nutrient to carbon ratios, but overall, the general trend is represented. The Spearman's rank correlation coefficient for C:N, N:P, and C:P are 0.30, 0.36, and 0.37, respectively. The model phytoplankton Fe:C ratios are compared to field observations of individual cell iron to carbon[100]. The Spearman's rank correlation coefficient for the phytoplankton community Fe:C is 0.30 (Fig. 2.1).

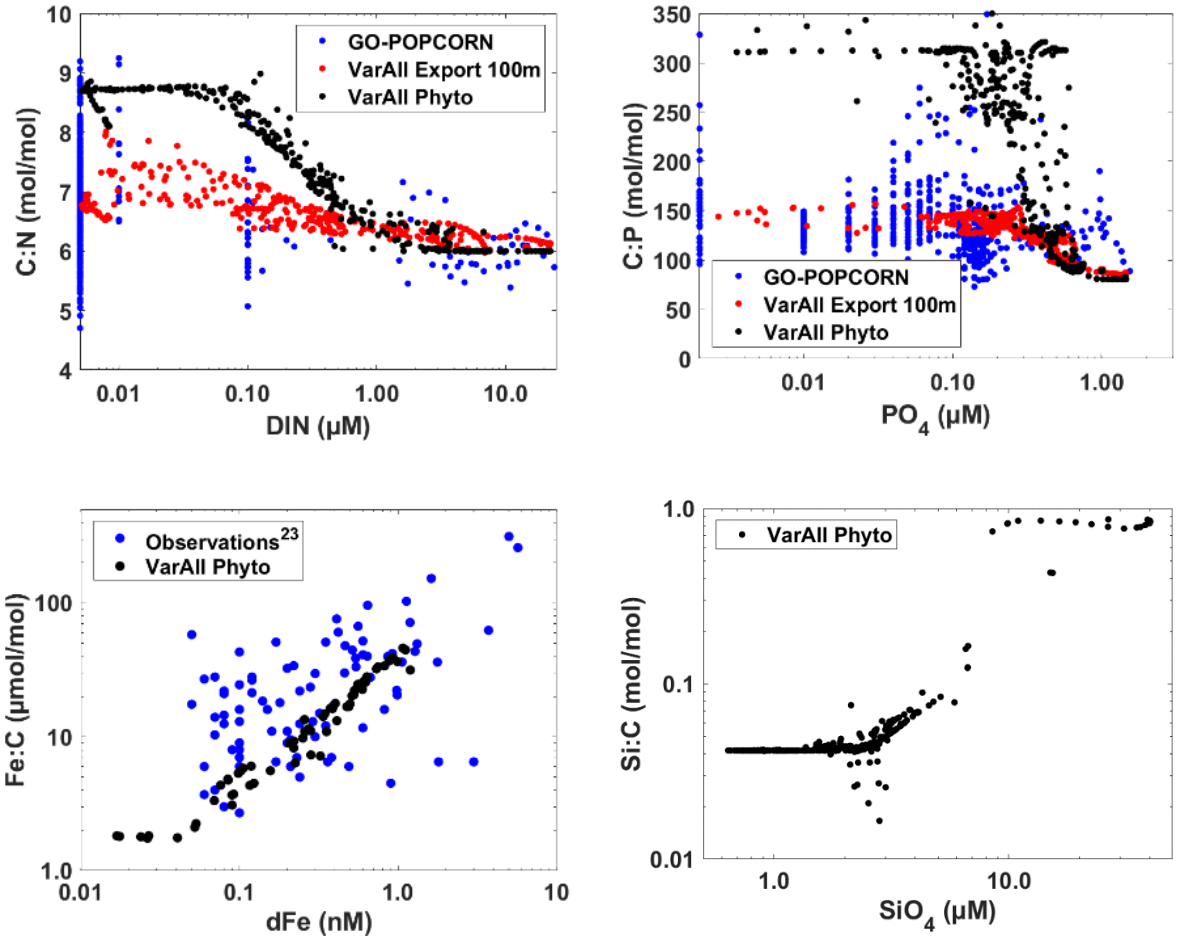

Figure 2.1. Simulated organic matter stoichiometry as a function of dissolved nutrient concentrations are compared with from observations from GO-POPCORNv2 and Wiseman et al., 2023[100]. Plots (a) and (b) show surface particulate organic matter C:N and C:P from GO-POPCORNv2 (blue) and model sinking export C:N and C:P at 100m (red) and phytoplankton community C:N and C:P (black). GO-POPCORNv2 observations are plotted against *in situ* measurements of total dissolved inorganic nitrate and nitrite (a) and dissolved phosphate (b), while model C:N and C:P is plotted against model dissolved inorganic nitrate and ammonia (a) and dissolved phosphate plus semi-labile dissolved organic phosphorus. Single cell Fe:C ratios are plotted against *in situ* dissolved iron concentrations (blue) and the model

community Fe:C ratios are compared with simulated dissolved iron (black). Simulated diatom Si:C ratios (d) are plotted against dissolved silicate concentrations. Model output was extracted from the same locations as the plotted observations.

Inverse models suggest elevated C:P ratios (> 140) and N:P ratios (>20) in the subtropical gyres, and much lower ratios of C:P (< 100) and N:P (< 16) in the regions with elevated surface phosphate concentrations (> 0.3 μM)[51,102]. Our model captures these large-scale patterns in C:N:P ratios of the sinking export flux (Fig. S2.2). The inferred global patterns are also broadly in agreement with the stoichiometry of surface POM in the POPCORN database. Combining the regional mean C:P and N:P in export estimated by these two inverse studies gives mean C:N of 8.5 for the North Pacific gyre, 6.7 for the South Pacific gyre, and 6.0 for the Southern Ocean (Figs. 2.1, 2.2, S2.2). Limited observations make evaluating the Si:C ratios more difficult. The model captures the observed patterns of elevated Si:C in iron-limited regions with elevated surface dSi concentrations, and the low Si:C seen under low Si conditions both *in situ* and in the laboratory[103–105]. Thus, our relatively simple approach, dynamically linking phytoplankton stoichiometry to ambient nutrient concentrations, captures the observed global-scale patterns in the stoichiometry of exported organic matter.

We compare a variable C:N:P:Fe:Si model simulation (VarAll) with a fixed-ratio model version (FixAll) to investigate how dynamic plankton stoichiometry influences marine biogeochemistry. We examine how incorporating dynamic phytoplankton stoichiometry affects the magnitude and spatial patterns of net primary production, sinking carbon export at 100m depth, nitrogen fixation, and water column denitrification.

The fully variable and fixed models have similar globally integrated NPP, but the FixAll simulation significantly underestimates POC export and key nitrogen cycle fluxes (N fixation and WC denitrification) (Fig. 2.2). The VarAll model has a total integrated NPP of 55 PgC/yr, POC Export at 100m of 7.8 PgC/yr, N fixation of 214 TgN/yr, and WC Denitrification of 57 TgN/yr, which are all within the range of previous satellite and model-based estimates[51,106,107]. When stoichiometry is fixed in the model, there are minimal changes to integrated NPP (+1%), but POC Export, N Fixation, and WC denitrification decrease by 10%, 24%, and 49%, respectively.

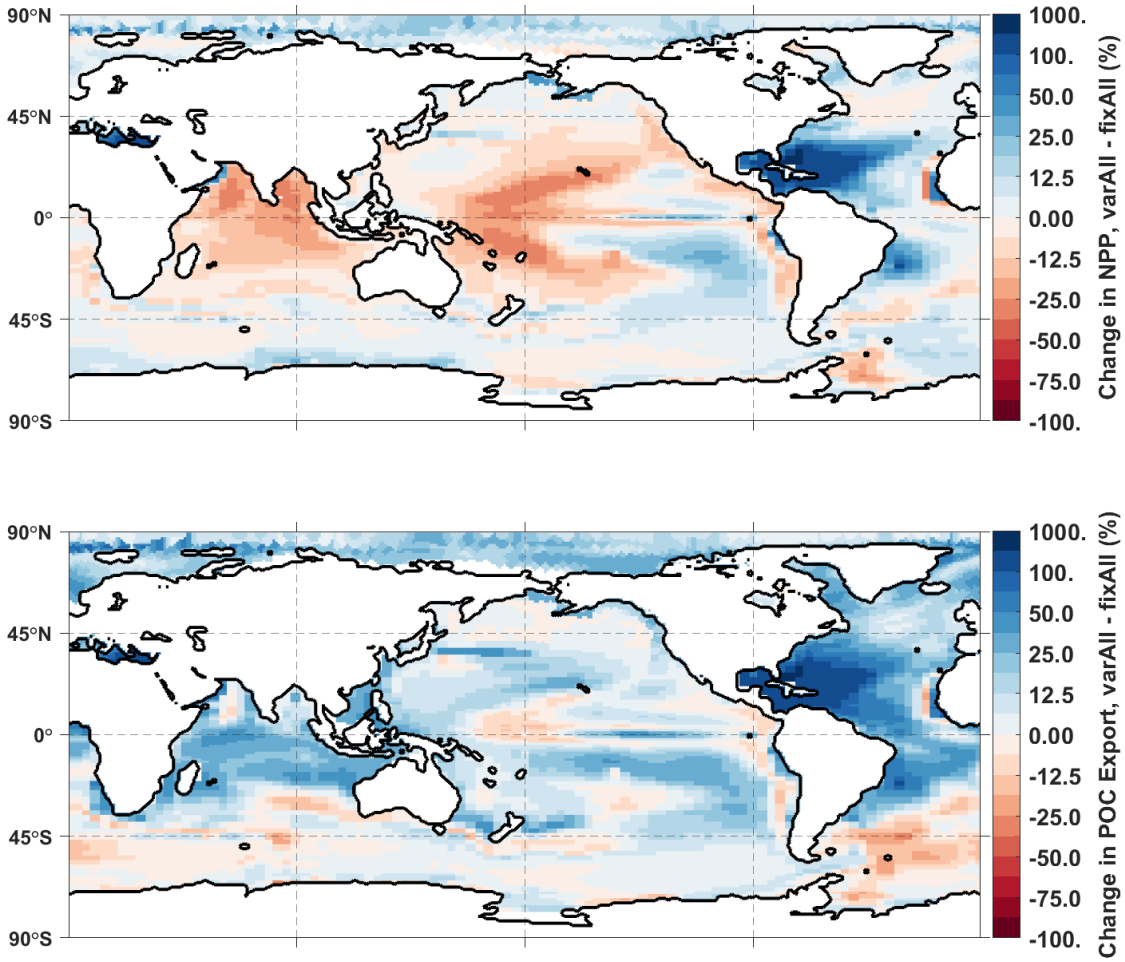

Figure 2.2. The differences between annual net primary production and sinking particulate carbon export comparing the VarAll - FixAll simulations.

The lower POC export in FixAll is driven by lower nutrient concentrations in surface waters but is enhanced by a community shift reducing diatom production and increasing the contribution from small phytoplankton in the more oligotrophic regions [22,108]. Export of the growth-limiting nutrient is always higher with fixed ratios, leading to increasing depletion and nutrient stress in surface waters, which favors the smaller phytoplankton. This shift also helps sustain NPP by decreasing export efficiency, leading to increasing regenerated production. The small phytoplankton are more efficient at nutrient uptake and are able to out-compete the diatoms under strongly, nutrient-limited conditions, such as in the Pacific and Indian gyres, where we see an increase in NPP and decreases in POC export in FixAll

compared to the VarAll case. The diatoms also have the additional limitation of Si availability, which causes them to have significant reductions in biomass in areas where Si is not readily available in the FixAll case. The only regions where diatoms have higher biomass in the FixAll case are in upwelling regions where Si is returned to the surface, such as the Southern Ocean and North Pacific. This suggests that diatom Si:C acclimation is critical for explaining the global distribution of diatoms, preventing Si-limitation of growth over much of the lower latitudes.

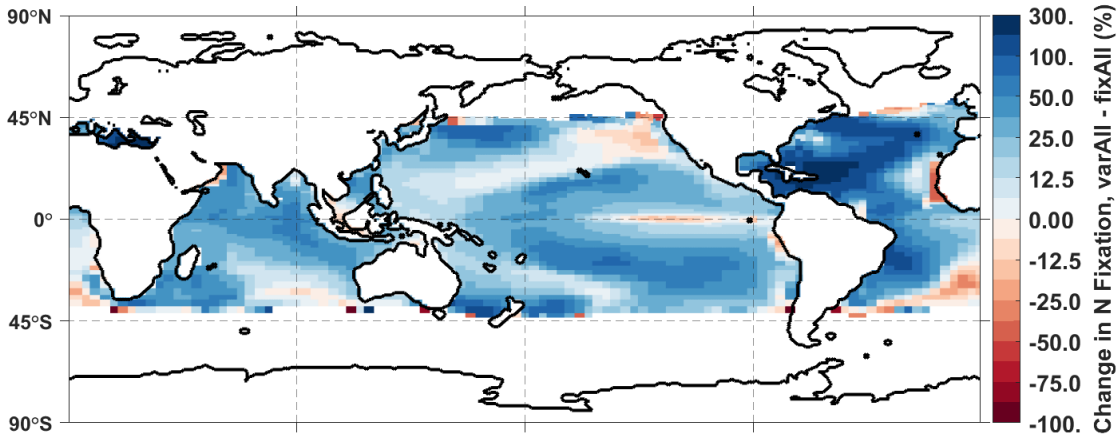

Figure 2.3. Differences in annual nitrogen fixation comparing the VarAll and FixAll simulations.

Nitrogen fixation and water column denitrification both decrease in FixAll in comparison to VarAll (Fig. 2.3). Nitrogen fixation decreases by up to 75% over much of the Atlantic Ocean and up to 25% in the Pacific Ocean, with a global decrease of 24% (Fig. 2.3). With fixed ratios, surface P declines in the North Atlantic and Indian basins and surface Fe declines over much of the Pacific. The declines in N fixation are largely due to increases in P and Fe stress. Nitrogen fixation rates in the North Atlantic are particularly dependent on P availability, and therefore decrease more drastically than in other regions [109]. The declines in N fixation also contribute to the decreasing POC export seen in many regions. Globally integrated water column denitrification decreases by 49%, with little change in the spatial pattern, due to decreases in diatom production and export over the Bay of Bengal and in the

eastern equatorial Pacific. The global volume of low oxygen (<30 mmol/m^3) waters decreases by 42%.

Both models are able to replicate observations of surface nutrients. When compared to World Ocean Atlas 2018, the R^2 for VarAll and surface NO_3, PO_4, and SiO_3 are 0.93, 0.91, and 0.74, respectively. For FixAll, these values are 0.92, 0.92, and 0.74 respectively[88]. For dissolved iron, we compare primarily to data collected from the GEOTRACES project, supplemented with historical data compilations[62,89,110]. The Spearman's rank correlation coefficient for dissolved iron is 0.45 for the VarAll model and 0.42 for the FixAll model.

Discussion

The relatively simple phytoplankton stoichiometry model presented here is able to capture the large-scale observed elemental stoichiometries. It is built around the frugal phytoplankton concept suggested by Galbraith and Martiny for plankton C:N:P ratios, whereby phytoplankton acclimate to increasing nutrient stress by decreasing the cellular quota of that nutrient[13]. Applying this concept to all the growth-limiting nutrients, with prescribed minimum and maximum nutrient:C ratios, allows for dynamic phytoplankton stoichiometry that captures the observed global patterns. The acclimation to low nutrient conditions strongly impacts the interactions between the biogeochemical cycles, modifying the strength and spatial patterns of the ocean biological pump.

We find that the coupling of biogeochemical cycles is strongly influenced by variable phytoplankton stoichiometry. Although it is possible to reproduce surface nutrient and net primary productivity distributions, the VarAll model utilizes additional observational constraints of surface nutrient stress and POM stoichiometric variability that are not otherwise captured by the FixAll model. This highlights the importance of using multiple observational constraints for marine ecosystem models in order to better capture complex interactions between the biogeochemical cycles.

For marine ecosystem and Earth System models to properly represent ocean carbon cycling in the context of climate change, it is imperative that they include variable phytoplankton stoichiometry. Fixed ratio models will overestimate the declines in NPP and export with increasing stratification, with biases in the spatial patterns of carbon export. The

globally integrated nitrogen fixation and water column denitrification are significantly lower in the FixAll model, which could lead to biases in bioavailable nitrogen, the primary limiting nutrient over much of the global ocean. These results stress the need for Earth System Models to capture the complexities of the cycling of nitrogen, phosphorus, iron, and silicon in the oceans, as they all influence and modify the strength and spatial patterns of the biological pump.

Methods

For this study, we used a modified version of CESM v1.2, which includes biogeochemical modifications that were introduced in CESM v2, including an explicit ligand, iron model[26,80]. The model includes three explicit phytoplankton groups (pico-nanophytoplankton, diatoms, and diazotrophs), one implicit group (coccolithophores, which are a variable fraction of the small phytoplankton group), and one zooplankton group [51,80]. For each simulation, the model was run at preindustrial CO_2 levels for 300 years using COREv2 interannual forcing, and we analyzed the output averaged over the last 20 years. This version of the model includes new equations and parameterization for phytoplankton nutrient quotas.

For each of the potentially growth-limiting nutrients, the stoichiometry for new phytoplankton growth (nutrient:C ratio) is a linear function of the ambient nutrient concentration, with prescribed minimum and maximum values (Fig. S1). This allows stoichiometry to dynamically adjust to changing environmental nutrient availability. Phytoplankton N:C ratios for new growth (gQn) are a function of dissolved inorganic nitrogen (DIN), which includes both nitrate and ammonia.

$$\mathrm{gQn} = \begin{cases} \mathrm{gQn\_max} & \text{where DIN} > \mathrm{NOpt} \\ \max\left(\mathrm{gQn\_max} \times \dfrac{\mathrm{DIN}}{\mathrm{NOpt}}, \mathrm{gQn\_min}\right) & \text{where DIN} < \mathrm{NOpt} \end{cases} \quad (1)$$

There are some modifications to the P:C formulation for new growth (gQp) in order to maintain appropriate N:P values as N:C ratios acclimate.

$$\mathrm{gQp} = \begin{cases} \mathrm{gQp\_max} & \text{where DIP} > \mathrm{POpt} \\ \max(\mathrm{gQp\_max} \times \dfrac{\mathrm{DIP}}{\mathrm{POpt}}, \mathrm{gQp\_min}) & \text{where DIP} < \mathrm{POpt} \\ \max(\mathrm{gQp\_max} \times \dfrac{\mathrm{DIN}}{\mathrm{NOpt}}, \mathrm{gQp\_min} \times \dfrac{\mathrm{gQn\_min}}{\mathrm{gQn\_max}}) & \text{where DIN} < \mathrm{NOpt} \end{cases} \quad (2)$$

$$\mathrm{gQfe} = \begin{cases} \mathrm{gQfe\_max} & \text{where dFe} > \mathrm{FeOpt} \\ \max(\mathrm{gQfe\_max} \times \dfrac{\mathrm{dFe}}{\mathrm{FeOpt}}, \mathrm{gQfe\_min}) & \text{where dFe} < \mathrm{FeOpt} \end{cases} \quad (3)$$

There are also modifications to the Si:C formulation in order to allow for diatoms to increase the Si:C uptake ratio when dFe is low.

$$\mathrm{gQsi} = \begin{cases} \begin{cases} \mathrm{gQsi\_max} & \text{where dFe} = 0 \\ \min(0.133 \times \dfrac{\mathrm{FeOpt}}{\mathrm{dFe}}, \mathrm{gQsi\_min}) & \text{where } 0 < \mathrm{dFe} < \mathrm{FeOpt} \\ 0.133 & \text{where dFe} > \mathrm{FeOpt} \end{cases} & \text{where } \mathrm{Si(OH)_4} > \mathrm{SiOpt} \\ \max(0.133 \times \dfrac{\mathrm{Si(OH)_4}}{\mathrm{SiOpt}}, \mathrm{gQsi\_min}) & \text{where } \mathrm{Si(OH)_4} > \mathrm{SiOpt} \end{cases}$$

Observations of particulate organic matter (POM) are from the GO-POPCORNv2 database[101]. Phytoplankton cellular iron to carbon ratios were previously compiled from multiple sources[100]. The parameters determined for each cellular nutrient ratio are provided (Table S2.1).

CHAPTER 3: Global patterns of nutrient limitation governed by phytoplankton stoichiometry

Introduction

Ocean carbon uptake is intrinsically linked to nutrient availability by phytoplankton stoichiometry, or the ratio between carbon and nutrients taken up by phytoplankton[13,14,99,111]. The ratio of phytoplankton carbon to nutrients has been shown to vary with growth rate, light availability, and nutrient limitation[13,14,99,111]. However, the processes controlling the spatial patterns and degree of nutrient limitation of phytoplankton growth rates are across poorly understood[22,27,112]. Nutrient limitation is a primary control on the export of carbon from surface waters into the ocean interior (the biological pump) and impacts the air-sea CO_2 flux and climate[113]. If we are to perform reliable simulations of the changing global carbon cycle under climate change, we must first understand the current controls on ocean carbon uptake.

A primary control on phytoplankton growth rate is nutrient availability, where certain nutrients are required by phytoplankton for photosynthesis and growth. Liebig's law of the minimum, which states that the single most limiting nutrient controls the growth capacity, has been the traditional theory behind phytoplankton nutrient limitation. However, in recent decades, the concept of co-limitation has been increasingly accepted where multiple nutrients in low concentrations can limit phytoplankton growth, particularly in the oligotrophic gyres[114].

Co-limitation has previously been described in three distinct forms[114]. The first is multi-nutrient co-limitation where the addition of more than one nutrient is required for growth. This may also come in the form of serial limitation, where when the primary limiting nutrient is added, the second most limiting nutrient becomes limiting, thereby requiring addition of both nutrients in order to stimulate growth. The second in biochemical co-limitation, where the addition of one nutrient can stimulate growth by aiding in the uptake of another limiting nutrient. The third is community co-limitation, where the addition of different nutrients induces growth of different species[114]. For example, addition of P to an N and P limited region can stimulate the growth of nitrogen fixers such as *Trichodesmium*,

which can then relieve N limitation of other phytoplankton groups. While much of the global oceans have previously been thought to be either N or Fe limited, further nutrient addition experiments have found evidence of N-Fe co-limitation[112]. However, the controls on large-scale patterns of nutrient limitation and what drives potential serial or co-limitation in different regions are not fully understood.

Understanding the controls of surface ocean nutrient limitation is key to understanding both past and future changes in ocean carbon uptake via the biological pump. The primary method for estimating nutrient limitation in the field is bottle incubation experiments, which are labor intensive and particularly difficult when multiple nutrients are required, or ambient concentrations are low[22,112,115]. Recent work utilized metagenomic analysis of *Prochlorococcus* stress genes to infer global patterns of nutrient stress, by nutrient type as well as severity[23]. Additionally, marine biogeochemical models can predict large scale patterns of nutrient limitation via the balance of nutrient supply to the surface ocean and the uptake by phytoplankton[27,52]. One advantage to marine biogeochemical models is that they can be used to perform global experiments where the marine ecosystem is perturbed in some way (regionally or functionally) to help further understand the connections between biogeochemical cycles and their downstream effects.

Earth system models are valuable tools for investigating the interactions between physics, biology, and biogeochemical cycles as they explicitly track individual nutrients, multiple phytoplankton functional types, and realistic ocean physics. Here, simulations with the Community Earth System Model (CESM) ocean component elucidate the interactions between varying phytoplankton stoichiometry and global ocean biogeochemistry. Simulations with and without varying stoichiometry demonstrate the role of variable phytoplankton nutrient acquisition on large-scale patterns of nutrient stress and the relative impacts of acclimation for each nutrient (N, P, Fe, Si).

We hypothesize that fixed stoichiometry for each individual nutrient will increase nutrient stress in oligotrophic regions, as phytoplankton will not be able to adapt to low nutrient availability by reducing cellular quotas. We also expect expansion of P limitation when phytoplankton are not allowed to vary their P:C stoichiometry. Phytoplankton have a

high P quota flexibility compared to N, so removing this flexibility could lead to an increase in the strength and areal extent of P limitation. But increasing P stress would limit the capacity for nitrogen fixation, that could otherwise alleviate N limitation, providing a potential negative feedback for expansion of P limitation. We also expect to see a distinct shift in community composition between the variable stoichiometry and fixed stoichiometry simulations, as smaller phytoplankton are able to out compete larger phytoplankton in the lower surface nutrient conditions that result from fixed phytoplankton stoichiometry, while diatoms would be further stressed by their inability to adjust their Si quotas.

To test these hypotheses, we compare a fully variable C:N:P:Fe:Si simulation with a fixed stoichiometry model simulation (for all nutrients and for each nutrient individually) to investigate how the cycling of each nutrient interacts and impacts nutrient limitation patterns and ecosystem structure. The CESM ocean module includes an ocean ecosystem and biogeochemistry model that contains three explicit phytoplankton groups (diatoms, pico-nanophytoplankton, a fraction of which acts as an implicit calcifier group, and diazotrophs) with variable nutrient quotas for phosphorus, iron, and silicon uptake[26,51]. The model has also recently been updated to include greater variability in the phytoplankton iron quotas as well as a new variable nitrogen quota parameterization. The new model simulates recreate realistic patterns of particulate organic matter stoichiometry and export, as well as surface nutrient concentrations and net primary productivity [100,113]. Phytoplankton progressively reduce their cellular nutrient quotas (nutrient:C ratios) under increasing nutrient stress (decreasing ambient concentrations)[100,113].

We analyze a series of simulations, the VarAll and FixAll simulations, have fully variable C:N:P:Fe:Si and fully fixed C:N:P:Fe:Si (in the phytoplankton and in the sinking export flux). Four experiments (FixN, FixP, FixFe, and FixSi) have variable stoichiometry with the exception of a single nutrient (N, P, Fe, and Si, respectively) and four experiments VarN, VarP, VarFe, and VarSi have fixed stoichiometry with the exception of a single nutrient. By examining the different responses in each of these experiments, we will disentangle the impacts of phytoplankton cycling of each nutrient on biogeochemical cycles. We will specifically look at the differences between each simulation for the magnitude and spatial

patterns of nutrient limitation and the phytoplankton community composition. Global scale fluxes and the dynamics of the biological pump have been studied previously for the VarAll and FixAll simulations[113].

Global Patterns of Nutrient Limitation

The VarAll simulation of nutrient limitation patterns is in excellent agreement with available *in situ* estimates of nutrient limitation. The model's spatial patterns of nutrient stress agree with estimates of nutrient stress from *in situ* nutrient-addition, bottle experiments for both the primary and secondary limiting nutrients (Fig. 3.1)[22].

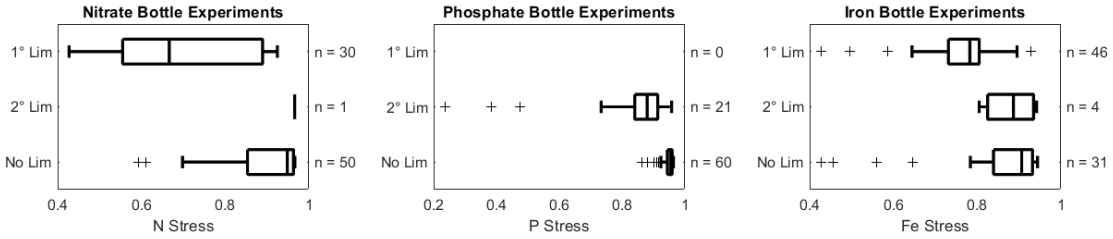

Figure 3.1. Degree of nutrient stress from the VarAll simulation (0-1, relative growth rate) compared to estimates from *in situ* nutrient addition bottle experiments (n = 81) for (**A**) nitrate, (**B**) phosphate, and (**C**) iron. Model output was extracted at the same locations as the *in situ* experiments and grouped by the degree of nutrient limitation in the bottle experiments. Stress factors are multiplied by a maximum growth rate and light and temperature factors to determine new growth in the model.

In areas where a nutrient is observed as either primary or secondary limiting, we see nutrient stress (decreases in relative growth due to nutrient stress) in our model for nitrate, phosphate, and iron. For example, at the locations where the bottle experiments determined N to be limiting, the model was also N limited, with on average about ~35% reduction in growth rate due to N availability (Fig. 3.1a). Compare this with the model output from the locations where N was determined not be limiting, the mean N nutrient stress factor was > 0.95 (Fig. 3.1a). The model also agrees with the bottle estimates of the degree of stress, where the model nutrient stress factor decreases from no limitation, to secondary limitation, to primary limitation (Fig. 3.1).

The VarAll simulation matches the large-scale spatial patterns of primary nutrient limitation observed from the bottle experiments (Figs. 3.1, 3.2)[22]. The gyres are primarily N limited for diatoms and pico-nanophytoplankton, and P limited for diazotrophs, with generally greater P stress in the North Atlantic. The HNLC regions are Fe limited for all phytoplankton groups. Diatoms experience Si limitation in limited regions, in high latitudes as well as in the eastern Atlantic. Diazotrophs are nutrient replete (grazer limited) in some regions (Fig. 3.2).

The model also agrees with observations of metagenomic nutrient stress, with N stress in the Indian Ocean, western Pacific, Atlantic gyres, P stress primarily in the North Atlantic, some in the Equatorial and South Atlantic, Fe stress over the majority of the Pacific Ocean, some in the south Indian ocean, and some in the high latitude North Atlantic (Fig. S3.1)[23]. In general, the gyres are characterized by moderate N stress. P stress is localized primarily in the western North Atlantic, with slight elevation along the western boundary current. Some Fe stress is found globally, except in regions of high iron supply, such as coastal shelves and in regions with high dust supply, such as beneath the Saharan and Asian dust plumes.

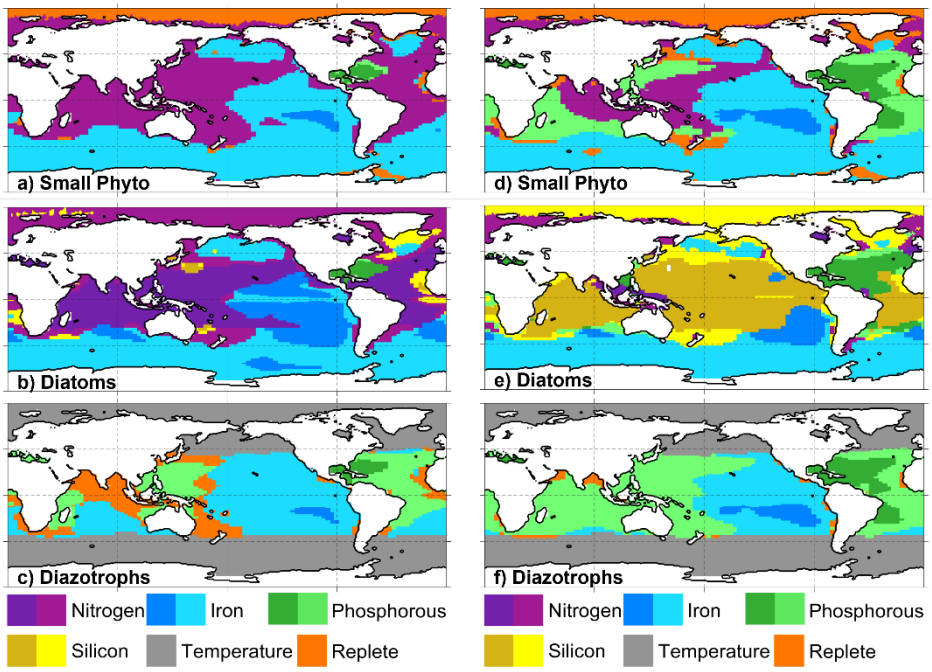

Figure 3.2. Patterns of nutrient limitation of (**a,d**) diatoms, (**b,e**) small phytoplankton, and (**c,f**) diazotrophs for the VarAll (a-c) and FixAll (d-f) simulations. Phytoplankton are nutrient replete when nutrient limitation reduces growth by less than 10%. Darker color shading indicates where growth is reduced by more than 50% due to nutrient availability.

The FixAll scenario has increases in P limitation for all groups, replacing mainly N limitation in the gyres (Fig. 3.2). The spatial pattern of Fe stress does not change significantly, and only strengthens slightly in the Pacific. For diatoms, Si limitation dominates (Fig. 3.2). These results suggest that the ability to acclimate to low nutrient availability by reducing cellular quotas is critical in preventing Si limitation for diatoms and P limitation for the community over much of the low latitudes. The potential flexibility in the N:C stoichiometry is much weaker than that for P:C, Fe:C, or Si:C. This acts to push marine ecosystems towards N limitation (VarAll simulation), as phytoplankton can better acclimate to low P, Fe, or Si, preventing their growth limitation. Only where the nutrient supply ratios are highly skewed can other nutrients become limiting. In the HNLC regions, the low iron inputs and the high inputs of N and P from below overwhelm the capacity of the phytoplankton to acclimate, making iron the primary limiting nutrient. High iron inputs to the North Atlantic spurs nitrogen fixation, depleting P to very low levels. Thus, surface nutrient concentrations and

patterns of nutrient limitation are set by the combined influence of the nutrient supply ratios and the stoichiometry of the exported organic matter (which varies dynamically as phytoplankton acclimate to changing nutrient conditions).

Results from the experiments where only one nutrient had a fixed or variable ratio provide further insights into these processes. Phytoplankton P quotas exert strong control on surface concentrations and the degree of P stress. When only P:C is fixed, the areal extent of P as the primary limiting nutrient expands from 2% of global ocean to 22%. The converse of adding variable P to fully fixed reduces P limitation from 12% to 2%. Si limitation shows a similar response, where Si limitation for diatoms jumps from 4% to 51% of global ocean when Si stoichiometry is fixed and reduces from 53% to 2% when variable. N and Fe do not show the same large responses. The N:C quota varies over a much smaller range than the other nutrients so fixing this ratio has less impact on surface nutrient distributions. The iron response and patterns of iron limitation are strongly tied to the external iron inputs to the oceans, which makes the spatial pattern of limitation less dynamic when considering fixed versus variable ratios.

When looking at the dynamic, degree of limitation across the different nutrients, we find that phytoplankton variable stoichiometry will also push marine ecosystems towards co-limitation over time. The non-growth limiting nutrients are initially exported at relatively high cellular quotas, making their export more efficient than that of the limiting nutrient (cellular quotas reduced). Over time this depletes the non-limiting nutrients, drawing the surface concentrations down towards growth-limiting concentrations. This pattern would not be expected in regions with regular nutrient injections (i.e., coastal upwelling zone) where there might not be time to draw down the non-limiting nutrients before resupply.

We calculated the limitation variance for each grid-cell, which is defined as the sum of the difference in the nutrient limitation growth factor of the growth-limiting nutrient (Eq. 3.1) and the other nutrients (Eq. 3.2). Therefore, a value closer to zero indicates that the non-limiting nutrients are approaching growth-limiting concentrations, giving nearly the same nutrient stress as seen in the primary limiting nutrient. We also calculated the co-limitation variance, which is the difference in relative growth rate between just the two most limiting nutrients (Eq. 3.3).

$$f_{lim} = min(f_N, f_P, f_{Fe}, f_{Si}) \quad \text{Eq. 3.1}$$

$$F_{tot} = \frac{1}{n}\sum_i^{N,P,Fe,Si} f_i - f_{lim} \quad \text{Eq. 3.2}$$

$$F_{\text{co}} = f_{2nd\ lim} - f_{lim} \quad \text{Eq. 3.3}$$

Comparing the nutrient limitation variances, F_{tot}, from the VarAll and FixAll simulations, for the diatom and diazotroph groups, variable stoichiometry pushes the mean values closer to zero, indicating that the non-primary limiting nutrients are being depleted and drawn down efficiently, often approaching growth-limiting concentrations (Fig. 3.3a). The FixAll simulations have more instances of higher F_{tot} values, indicating that non-limiting nutrients are not being drawn down as efficiently compared to the VarAll simulation. Looking at just the two most limiting nutrients pushes the distribution of F_{co} values closer to zero for both cases, indicating a significant amount of co-limitation, or near co-limitation, occurring (Fig. 3.3b).

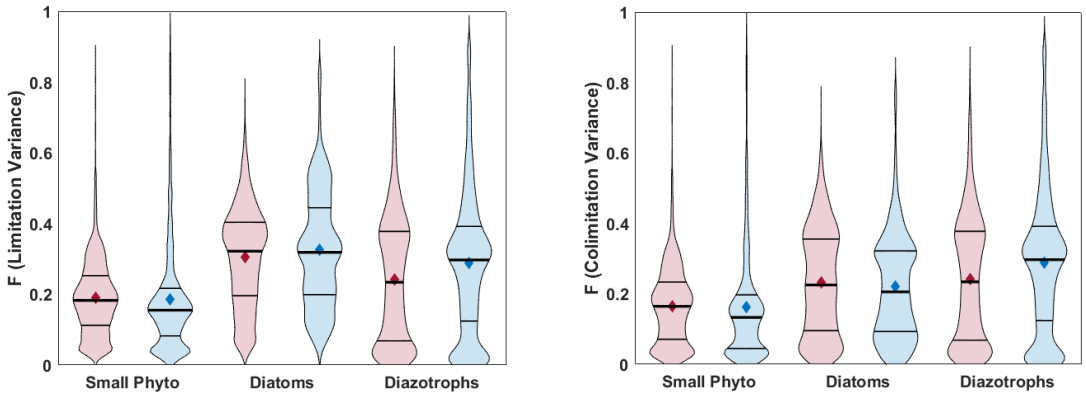

Figure 3.3. Limitation variance for each phytoplankton group. Violin plot for (**A**) total limitation variance and (**B**) colimitation variance for each phytoplankton group. Violin thickness corresponds to probability density, with thin black lines at 25th and 75th percentiles, thick black line at median, and diamond at mean value. VarAll model is shown in red, FixAll model is shown in black. Small phytoplankton can be N, P, or Fe limited, diatoms can be N, P, Fe, or Si limited, and diazotrophs can be either Fe or P limited.

Isolating each nutrient individually highlights the nonlinear responses to individual nutrient variability. For example, when N:C and P:C are fixed, their globally integrated export fluxes increase, while when Fe and Si are fixed, their globally integrated export fluxes

decrease (Table 3.1). The opposite is true when the nutrients are allowed to vary in an otherwise fixed model, with variable N and P leading to decreases in total integrated N and P export, and variable Fe and Si leading to increases in total integrated Fe and Si export. This is likely due to the spatial patterns of variability for each nutrient and the fixed value that is set, where regions that typically have higher nutrient:C ratios than the fixed value see reductions in export of that nutrient while regions that typically have lower nutrient:C ratios than the fixed value see increases in export of that nutrient. This highlights the uncertainty that can be introduced into models when a fixed nutrient:C ratio is used, as it leads to regional biases in export fluxes, and potentially globally as well[113].

Diatom Si variability strongly influences the global community composition to favor small phytoplankton over both diatoms and diazotrophs. When Si is fixed, export of all nutrients decreases globally as diatoms are displaced by small phytoplankton (a group that exports less efficiently). Interestingly, diazotroph biomass is also linked to Si variability, decreasing by 9% with Si is fixed, and increasing by 11% when Si is allowed to vary. The primary regions of reduction in diazotroph biomass are also where small phytoplankton see some of the greatest increases, specifically in the western Pacific and in the Indian Ocean (Fig. S3.2). There are also strong decreases in diazotroph biomass near their thermal limit, where fast growing small phytoplankton are easily able to outcompete them for resources (Fig. S3.2). Although diazotrophs and small phytoplankton do not rely on Si uptake for growth, they are still impacted by perturbations to Si cycling due to community interactions.

Table 3.1. Impacts of individual nutrients on globally integrated carbon biomass and nutrient export (sinking flux at 100m). White indicates <1% change, lightest color indicates 1%-4% change, middle color indicates 5%-9% changes, darkest color indicates >10% change, with red being negative change and blue being positive change.

	Total Biomass	Small Biomass	Diatom Biomass	Diaz Biomass	C Export	N Export	P Export	Fe Export	Si Export
VarAll									
FixN	-5	-3	-7	-1	0	+4	-2	+1	+1
FixP	+3	+2	+3	0	-9	-9	+7	-2	-1
FixFe	+1	-4	+4	+2	0	0	-2	-6	+3
FixSi	-3	+31	-33	-9	-6	-5	-9	-5	-13
FixAll									
VarN	+3	+3	+1	0	0	-2	0	0	-1
VarP	-1	-1	-2	+1	+5	+4	-8	0	0
VarFe	0	+2	-4	0	0	0	0	+6	-5
VarSi	+2	-25	+43	+11	+4	+6	+6	+4	+14

Discussion

We find that phytoplankton variable stoichiometry controls patterns of phytoplankton nutrient limitation and that individual nutrients have distinct roles. Export ratios from the euphotic zone are driven by phytoplankton stoichiometry and may act in opposite of nutrient supply ratios. It is the balance between these two that sets nutrient limitation patterns. The oceans are primarily N limited due to the weaker flexibility of phytoplankton N:C stoichiometry. The only regions where N is not the primary limiting nutrient is where nutrient supply ratios are highly skewed, such as in the HNLC regions where iron supply is much lower than nitrogen or phosphorus inputs, or in the North Atlantic, where substantial iron supply and nitrogen fixation lead to P limitation [116]. We also show that non-growth limiting nutrients are drawn down by variable nutrient acquisition over time, promoting serial or co-limitation.

The CMIP6 model ensemble has a significantly large spread in estimate of total carbon export and do not agree in how the biological pump will change under future climate scenarios[20]. Many of these models still do not include fully variable stoichiometry and may have limited phytoplankton diversity[19]. This heterogeneity in marine ecosystem representation may explain some of the divergence in biological pump strength within the CMIP6 ensemble. The location and amount of carbon export occurring within the ocean is important for nitrogen cycling and therefore nutrient availability. With variable nutrient acquisition, phytoplankton are able to acclimate to low nutrient conditions in order to maintain growth. This acclimation may prove to particularly useful in a warmer ocean as nutrient supply may diminish with changing circulation[79,94]. Not only does reducing their nutrient:C ratios help phytoplankton acclimate to nutrient stress, but it also increases the carbon export efficiency of the biological pump and could help buffer future reductions in net primary productivity[18,102].

Materials and Methods

For this study, we used a modified version of the Community Earth System Model (CESM1.2), which includes modifications that were introduced in CESM v2.0, including an explicit ligand, iron model[26,80]. CESM includes three explicit phytoplankton groups (nanophytoplankton, diatoms, and diazotrophs), one implicit group (coccolithophores, which are a fraction of the small phytoplankton group), and one zooplankton group[51,80]. For each simulation, the model was run at preindustrial CO_2 for 300 years using COREv2 interannual forcing, with the output averaged over the last 20 years. The nutrient to carbon ratio (quota) for new phytoplankton growth is determined by ambient nutrient concentrations in a linear manner, with minimum and maximum cellular quotas prescribed[113]. The parameters determined for each cellular nutrient ratio are provided (Table 3.2). To elucidate the impacts of each nutrient ratio on biogeochemical cycling, we iterated experiments where we fixed each individual nutrient ratio (N, P, Fe, Si) while allowing the others to vary, and also varied each nutrient while keeping the others fixed. The variable stoichiometry potential ranges and fixed values are provided (Table 3.3). The FixAll and VarAll simulations have been analyzed previously in terms of key biogeochemical fluxes and the impacts on the biological pump[113].

Table 3.2. Model parameters for determining phytoplankton nutrient quotas for new growth. xOpt refers to the nutrient concentration (for each nutrient) above which the maximum ratio (gQx_max) is used, and gQx_min is the minimum ratio applied at low nutrient concentrations[113].

	Picophytoplankton	Diatoms	Diazotrophs
NOpt, gQn_min, gQn_max	0.4, 0.111, 0.167	0.4, 0.111, 0.167	0.4, 0.143, 0.167
POpt, gQp_min[1], gQp_max	1.0, 0.004, 0.013	1.0, 0.008, 0.011	1.0, 0.004, 0.008
FeOpt, gQfe_min, gQfe_max	1.3, 3.0, 90.0	1.3, 3.0, 90.0	1.6, 4.5, 135.0
SiOpt, gQsi_min, gQsi_max	N/A		N/A

[1]P:C minimum quotas can be reduced to a smaller value due to the N:P scaling

Table 3.3. Potential range of stoichiometric variability for each nutrient for each phytoplankton group. All values given in units of mol/mol except Fe:C which is in units of μmol/mol. In the simulations where stoichiometry is fixed, the fixed value is applied to all phytoplankton groups.

	Pico-nano phytoplankton	Diatoms	Diazotrophs	Fixed
C:N	6-9	6-9	6-7	6
N:P	13.3-37.5	15-20	20-45	16
C:P	80-225 (337.5)	90-120 (180)	120-270 (315)	96
Fe:C	3-90	3-90	4.5-135	7
Si:N		0.25-4.0		1

CHAPTER 4: Summary and Conclusions

The overarching goal of my thesis was two-fold: to implement variable stoichiometry within the Community Earth System Model ocean component informed by field observations, and to use this model to investigate the roles of phytoplankton stoichiometry as a whole and of individual nutrients to further understand the interactions between biogeochemical cycles within the ocean.

In my first chapter, I modified the Community Earth System Model ocean component to simulate dynamic, group-specific, phytoplankton Fe:C that varied as a function of ambient iron concentration. This new parameterization for phytoplankton Fe:C ratios improved the model's ability to capture spatial trends from *in situ* observations. I found that acclimation of phytoplankton Fe:C ratios dampened the biogeochemical response to varying atmospheric deposition of soluble iron, compared to a fixed Fe:C ratio. However, varying atmospheric soluble iron supply had first order impacts on global carbon and nitrogen fluxes, and on nutrient limitation spatial patterns. My results suggest that pyrogenic Fe is a significant dFe source that rivals mineral dust inputs in some regions. Accounting for dynamic phytoplankton iron quotas is critical for understanding ocean biogeochemistry and projecting its response to variations in atmospheric deposition as dust fluxes and iron combustion sources (anthropogenic and wildfires) modify atmospheric Fe inputs in the future.

In my second chapter, I implemented a variable nitrogen quota for phytoplankton growth and showed that the modified ocean model captures observed correlations between variable plankton elemental stoichiometry and ambient nutrient concentrations, with decreasing cellular nutrient quotas under increasing nutrient stress. I found that accurate representation of phytoplankton elemental stoichiometry, which links the cycling of carbon and key growth-limiting nutrients, is critical to simulate the strength and spatial patterns of carbon export by the biological pump, and for understanding how it will respond to climate change. This further supports that Earth System Models need to include dynamic plankton stoichiometry and reproduce the observed, low-nutrient conditions in oligotrophic regions, in order to accurately project climate feedbacks involving the biological pump.

Lastly, I used the modified model to find that phytoplankton acclimate to increasing nutrient stress by decreasing their nutrient:carbon ratios. When phytoplankton reduce their cellular quotas, they reduce the export efficiency of the limiting nutrient, helping sustain biological productivity. I found that surface nutrient concentrations and patterns of nutrient limitation are a function of the nutrient supply ratios and the elemental ratios in the exported organic matter, which is driven by variable phytoplankton stoichiometry. The weaker ability of phytoplankton to acclimate to N stress by lowering their cellular quotas relative to other nutrients pushes marine ecosystems towards nitrogen limitation. Only when the nutrient supply ratios are highly skewed, exceeding the ability of the phytoplankton to acclimate, do other nutrients become growth-limiting, as with iron in the High Nitrate, Low Chlorophyll (HNLC) regions. I also showed that variable plankton stoichiometry, given sufficient time, will also push marine ecosystems towards co-limitation, as non-limiting nutrient are more efficiently drawn down and exported, relative to the growth-limiting nutrient.

Overall, the work that I have done furthers our understanding of the interaction between phytoplankton stoichiometry and global nutrient cycles. It is clear that variable phytoplankton quotas allow them to acclimate to changes in nutrient stress in order to sustain growth. As marine biogeochemical cycles are perturbed by anthropogenic forcing, this acclimation will likely become important in buffering the impacts of reduced nutrient availability on the strength of the biological pump. Further work should focus on the impacts of variable phytoplankton quotas within climate simulations, as I would expect that this acclimation will help phytoplankton sustain some level of carbon export even when nutrient supply is reduced by enhanced stratification.

Another point of further research should be looking into how variable phytoplankton quotas interact with proposed methods of marine carbon dioxide removal, particularly those that involve perturbing the biological pump. For example, luxury storage of iron by phytoplankton could reduce the efficiency of carbon export in iron fertilization experiments, thereby making it less cost effective (more iron required for substantial carbon export for long term removal). Conversely, phytoplankton resource acclimation could also help reduce the negative impacts of "nutrient robbing" where biological pump stimulation in one region reduces the available nutrients for growth downstream. Any perturbations to the biological

pump must account for these variable quotas as part of proposed MRV (measurement, reporting and verification) in order to truly quantify the amount of carbon exported by marine carbon dioxide removal efforts.

Lastly, I want to highlight the importance of *in situ* observations in informing earth system models for climate simulations. It is not enough for ocean models to only simulate surface nutrients and chlorophyll, and additional metrics such as phytoplankton and particulate organic matter stoichiometry can help ensure that ocean models are accurately representing the complex interactions between biogeochemical cycles. Even the observations used throughout my work do not fully capture the heterogeneity of the global oceans, and efforts should continue to be made to improve the spatial distribution of *in situ* data. This work would not have been possible without such measurements in addition to sustained observations of surface nutrients.

References

1. Friedlingstein, P. *et al.* Global carbon budget 2019. *Earth Syst Sci Data* **11**, 1783–1838 (2019).

2. Volk, T. & Hoffert, M. I. Ocean carbon pumps: Analysis of relative strengths and efficiencies in ocean-driven atmospheric CO2 changes. in *The Carbon Cycle and Atmospheric CO2 : Natural Variations Archean to Present* vol. 32 99–110 (American Geophysical Union, 2013).

3. Le Quéré, C. *et al.* Ecosystem dynamics based on plankton functional types for global ocean biogeochemistry models. *Glob. Chang. Biol.* **11**, 2016–2040 (2005).

4. Mills, M. M., Ridame, C., Davey, M., La Roche, J. & Geider, R. J. Iron and phosphorus co-limit nitrogen fixation in the eastern tropical North Atlantic. *Nature* **429**, 292–294 (2004).

5. Moore, J. & Doney, S. C. Iron availability limits the ocean nitrogen inventory stabilizing feedbacks between marine denitrification and nitrogen fixation. *Global Biogeochem. Cycles* **21**, (2007).

6. Tyrrell, T. The relative influences of nitrogen and phosphorus on oceanic primary production. *Nature* **400**, 525–531 (1999).

7. Bruland, K. W., Donat, J. R. & Hutchins, D. A. Interactive influences of bioactive trace metals on biological production in oceanic waters. *Limnol. Oceanogr.* **36**, 1555–1577 (1991).

8. Redfield, A. C., Ketchum, B. C. & Richards, F. A. The influence of organisms on the composition of sea water. in *The Sea* (ed. Hill, N.) vol. 2 26–77 (Wiley Intersci., 1963).

9. Schneider, B., Engel, A. & Schlitzer, R. Effects of depth-and CO2-dependent C: N ratios of particulate organic matter (POM) on the marine carbon cycle. *Global Biogeochem. Cycles* **18**, (2004).

10. Martiny, A. C. *et al.* Strong latitudinal patterns in the elemental ratios of marine plankton and organic matter. *Nat. Geosci.* **6**, 279–283 (2013).

11. Twining, B. S., Baines, S. B. & Fisher, N. S. Element stoichiometries of individual plankton cells collected during the Southern Ocean Iron Experiment (SOFeX). *Limnol. Oceanogr.* **49**, 2115–2128 (2004).

12. Weber, T. S. & Deutsch, C. Ocean nutrient ratios governed by plankton biogeography. *Nature* **467**, 550–554 (2010).

13. Galbraith, E. D. & Martiny, A. C. A simple nutrient-dependence mechanism for predicting the stoichiometry of marine ecosystems. *Proc. Natl. Acad. Sci. U. S. A.* **112**, 8199–8204 (2015).

14. Tanioka, T. & Matsumoto, K. A meta-analysis on environmental drivers of marine phytoplankton C: N: P. *Biogeosciences* (2020).

15. Kwiatkowski, L., Aumont, O., Bopp, L. & Ciais, P. The Impact of Variable Phytoplankton Stoichiometry on Projections of Primary Production, Food Quality, and Carbon Uptake in the Global Ocean. *Global Biogeochem. Cycles* **32**, 516–528 (2018).

16. Buchanan, P. J., Matear, R. J., Chase, Z., Phipps, S. J. & Bindoff, N. L. Dynamic Biological Functioning Important for Simulating and Stabilizing Ocean Biogeochemistry. *Global Biogeochem. Cycles* **32**, 565–593 (2018).

17. Tanioka, T. & Matsumoto, K. Buffering of ocean export production by flexible elemental stoichiometry of particulate organic matter. *Global Biogeochem. Cycles* **31**, 1528–1542 (2017).

18. Kwon, E. Y. *et al.* Nutrient uptake plasticity in phytoplankton sustains future ocean net primary production. *Sci Adv* **8**, eadd2475 (2022).

19. Séférian, R. *et al.* Tracking Improvement in Simulated Marine Biogeochemistry Between CMIP5 and CMIP6. *Curr Clim Change Rep* **6**, 95–119 (2020).

20. Henson, S. A. *et al.* Uncertain response of ocean biological carbon export in a changing world. *Nat. Geosci.* **15**, 248–254 (2022).

21. Tanioka, T. *et al.* Global Ocean Particulate Organic Phosphorus, Carbon, Oxygen for Respiration, and Nitrogen (GO-POPCORN). *Sci Data* **9**, 688 (2022).

22. Moore, C. M. *et al.* Processes and patterns of oceanic nutrient limitation. *Nat. Geosci.* **6**, 701–710 (2013).

23. Ustick, L. J. *et al.* Metagenomic analysis reveals global-scale patterns of ocean nutrient limitation. *Science (1979)* **372**, 287–291 (2021).

24. Twining, B. S., Rauschenberg, S. & Morton Peter L and Vogt, S. Metal contents of phytoplankton and labile particulate material in the North Atlantic Ocean. *Prog. Oceanogr.* **137**, 261–283 (2015).

25. Boyd, P. W. *et al.* Mesoscale iron enrichment experiments 1993-2005: synthesis and future directions. *Science (1979)* **315**, 612–617 (2007).

26. Moore, J. K., Doney, S. C. & Lindsay, K. Upper ocean ecosystem dynamics and iron cycling in a global three-dimensional model. *Global Biogeochem. Cycles* **18**, (2004).

27. Moore, J. K., Doney, S. C., Glover, D. M. & Fung, I. Y. Iron cycling and nutrient-limitation patterns in surface waters of the World Ocean. *Deep Sea Res. Part 2 Top. Stud. Oceanogr.* **49**, 463–507 (2002).

28. Buchanan, P. J., Chase, Z., Matear, R. J., Phipps, S. J. & Bindoff, N. L. Marine nitrogen fixers mediate a low latitude pathway for atmospheric CO2 drawdown. *Nat. Commun.* **10**, 4611 (2019).

29. Falkowski, P. G. Evolution of the nitrogen cycle and its influence on the biological sequestration of CO2 in the ocean. *Nature* **387**, 272–275 (1997).

30. Fung, I. Y. *et al.* Iron supply and demand in the upper ocean. *Global Biogeochem. Cycles* **14**, 281–295 (2000).

31. King, A. L. *et al.* A comparison of biogenic iron quotas during a diatom spring bloom using multiple approaches. *Biogeosciences* **9**, 667–687 (2012).

32. Hamilton, D. S. *et al.* Recent (1980 to 2015) trends and variability in daily-to-interannual soluble iron deposition from dust, fire, and anthropogenic sources. *Geophys. Res. Lett.* **47**, (2020).

33. Ho, T.-Y. *et al.* The elemental composition of some marine phytoplankton. *J. Phycol.* **39**, 1145–1159 (2003).

34. Martin, J. H. & Knauer, G. A. The elemental composition of plankton. *Geochim. Cosmochim. Acta* **37**, 1639–1653 (1973).

35. Schmidt, M. A. & Hutchins, D. A. Size-fractionated biological iron and carbon uptake along a coastal to off shore transect in the NE Pacific. *Deep-Sea Research II* **46**, 2487 (1999).

36. Sunda, W. G. & Huntsman, S. A. Iron uptake and growth limitation in oceanic and coastal phytoplankton. *Mar. Chem.* **50**, 189–206 (1995).

37. Twining, B. S. *et al.* Quantifying trace elements in individual aquatic protist cells with a synchrotron X-ray fluorescence microprobe. *Anal. Chem.* **75**, 3806–3816 (2003).

38. Marchetti, A. & Maldonado, M. T. Iron. in *The physiology of Microalgae* (eds. Borowitzka, M., Beardall, J. & Ravel, J.) vol. 6 233–279 (Springer, Cham, 2016).

39. Sunda, W. G., Swift, D. G. & Huntsman, S. A. Low iron requirement for growth in oceanic phytoplankton. *Nature* **351**, 55–57 (1991).

40. Marchetti, A. *et al.* Ferritin is used for iron storage in bloom-forming marine pennate diatoms. *Nature* **457**, 467–470 (2009).

41. Twining, B. S. *et al.* Taxonomic and nutrient controls on phytoplankton iron quotas in the ocean. *Limnol. Oceanogr. Lett.* **6**, 96–106 (2021).

42. Hudson, R. J. M. & Morel, F. M. M. Iron transport in marine phytoplankton: Kinetics of cellular and medium coordination reactions. *Limnol. Oceanogr.* **35**, 1002–1020 (1990).

43. Morel, F. M. M., Hudson, R. J. M. & Price, N. M. Limitation of productivity by trace metals in the sea. *Limnol. Oceanogr.* **36**, 1742–1755 (1991).

44. Twining, B. S., Baines, S. B. & Fisher Nicholas S and Landry, M. R. Cellular iron contents of plankton during the Southern Ocean Iron Experiment (SOFeX). *Deep Sea Res. Part I* **51**, 1827–1850 (2004).

45. Kazamia, E. *et al.* Endocytosis-mediated siderophore uptake as a strategy for Fe acquisition in diatoms. *Sci Adv* **4**, eaar4536 (2018).

46. Berman-Frank, I., Cullen, J. T., Shaked, Y., Sherrell, R. M. & Falkowski, P. G. Iron availability, cellular iron quotas, and nitrogen fixation in Trichodesmium. *Limnol. Oceanogr.* **46**, 1249–1260 (2001).

47. Howard, J. B. & Rees, D. C. Structural Basis of Biological Nitrogen Fixation. *Chem. Rev.* **96**, 2965–2982 (1996).

48. Sañudo-Wilhelmy, S. A. *et al.* Phosphorus limitation of nitrogen fixation by Trichodesmium in the central Atlantic Ocean. *Nature* **411**, 66–69 (2001).

49. Buesseler, K. O. The decoupling of production and particulate export in the surface ocean. *Global Biogeochem. Cycles* **12**, 297–310 (1998).

50. Hamilton, D. S. *et al.* Impact of changes to the atmospheric soluble iron deposition flux on ocean biogeochemical cycles in the anthropocene. *Global Biogeochem. Cycles* **34**, e2019GB006448 (2020).

51. Wang, W.-L., Moore, J. K., Martiny, A. C. & Primeau, F. W. Convergent estimates of marine nitrogen fixation. *Nature* **566**, 205–211 (2019).

52. Krishnamurthy, A., Moore, J. K., Mahowald Natalie and Luo, C. & Zender, C. S. Impacts of atmospheric nutrient inputs on marine biogeochemistry. *J. Geophys. Res.* **115**, (2010).

53. Hopkinson, B. M. *et al.* Planktonic C:Fe ratios and carrying capacity in the southern Drake Passage. *Deep Sea Res. Part 2 Top. Stud. Oceanogr.* **90**, 102–111 (2013).

54. Twining, B. S. *et al.* A nutrient limitation mosaic in the eastern tropical Indian Ocean. *Deep Sea Res. Part 2 Top. Stud. Oceanogr.* **166**, 125–140 (2019).

55. Moreno, A. R., Hagstrom, G. I., Primeau Francois W and Levin, S. A. & Martiny, A. C. Marine phytoplankton stoichiometry mediates nonlinear interactions between nutrient supply, temperature, and atmospheric CO2. *Biogeosciences* **15**, (2018).

56. Weber, T. & Deutsch, C. Oceanic nitrogen reservoir regulated by plankton diversity and ocean circulation. *Nature* **489**, 419–422 (2012).

57. Buitenhuis, E. T. & Geider, R. J. A model of phytoplankton acclimation to iron-light colimitation. *Limnol. Oceanogr.* **55**, 714–724 (2010).

58. Aumont, O., Ethé, C., Tagliabue, A., Bopp, L. & Gehlen, M. PISCES-v2: an ocean biogeochemical model for carbon and ecosystem studies. *Geosci. Model Dev.* **8**, 2465–2513 (2015).

59. Tagliabue, A. *et al.* An iron cycle cascade governs the response of equatorial Pacific ecosystems to climate change. *Glob. Chang. Biol.* (2020).

60. Person, R., Aumont, O. & Lévy, M. The biological pump and seasonal variability of pCO 2 in the southern ocean: Exploring the role of diatom adaptation to low iron. *J. Geophys. Res. C: Oceans* **123**, 3204–3226 (2018).

61. Tagliabue, A. *et al.* The integral role of iron in ocean biogeochemistry. *Nature* **543**, 51–59 (2017).

62. Moore, J. K. & Braucher, O. Sedimentary and mineral dust sources of dissolved iron to the world ocean. *Biogeosciences* **5**, 631–656 (2008).

63. Mahowald, N. M. *et al.* Desert dust and anthropogenic aerosol interactions in the Community Climate System Model coupled-carbon-climate model. *Biogeosciences* **8**, 387–414 (2011).

64. Tagliabue, A. *et al.* How well do global ocean biogeochemistry models simulate dissolved iron distributions? *Global Biogeochem. Cycles* **30**, 149–174 (2016).

65. Archer, D. E. & Johnson, K. A model of the iron cycle in the ocean. *Global Biogeochem. Cycles* **14**, 269–279 (2000).

66. Bopp, L., Kohfeld, K. E. & Le Quéré Corinne and Aumont, O. Dust impact on marine biota and atmospheric CO2during glacial periods. *Paleoceanography* **18**, (2003).

67. Jickells, T. D. & Spokes, L. J. Atmospheric iron inputs to the oceans. in *The Biogeochemistry of Iron in Seawater* vol. SCOR/IUPAC Series 85–121 (Wiley, 2001).

68. Lefèvre, N. & Watson, A. J. Modeling the geochemical cycle of iron in the oceans and its impact on atmospheric CO2concentrations. *Global Biogeochem. Cycles* **13**, 727–736 (1999).

69. Mahowald, N. M. *et al.* Atmospheric iron deposition: global distribution, variability, and human perturbations. *Ann. Rev. Mar. Sci.* **1**, 245–278 (2009).

70. Wu, J. & Boyle, E. Iron in the Sargasso Sea: Implications for the processes controlling dissolved Fe distribution in the ocean. *Global Biogeochem. Cycles* **16**, 33–1–33–8 (2002).

71. Ito, A. *et al.* Pyrogenic iron: The missing link to high iron solubility in aerosols. *Sci Adv* **5**, eaau7671 (2019).

72. Matsui, H. *et al.* Anthropogenic combustion iron as a complex climate forcer. *Nat. Commun.* **9**, 1593 (2018).

73. Sedwick, P. N., Sholkovitz, E. R. & Church, T. M. Impact of anthropogenic combustion emissions on the fractional solubility of aerosol iron: Evidence from the Sargasso Sea. *Geochem. Geophys. Geosyst.* **8**, (2007).

74. Ito, A., Ye, Y., Yamamoto, A., Watanabe, M. & Aita, M. N. Responses of ocean biogeochemistry to atmospheric supply of lithogenic and pyrogenic iron-containing aerosols. *Geol. Mag.* **157**, 741–756 (2020).

75. Myriokefalitakis, S. *et al.* Reviews and syntheses: the GESAMP atmospheric iron deposition model intercomparison study. *Biogeosciences* **15**, 6659–6684 (2018).

76. Conway, T. M. *et al.* Tracing and constraining anthropogenic aerosol iron fluxes to the North Atlantic Ocean using iron isotopes. *Nat. Commun.* **10**, 2628 (2019).

77. Hamilton, D. S. *et al.* Earth, Wind, Fire, and Pollution: Aerosol Nutrient Sources and Impacts on Ocean Biogeochemistry. *Ann. Rev. Mar. Sci.* **14**, 303–330 (2022).

78. Lamb, K. D. *et al.* Global-scale constraints on light-absorbing anthropogenic iron oxide aerosols. *NPJ Clim Atmos Sci* **4**, 1–12 (2021).

79. Liu, Y., Moore, J. K., Primeau, F. & Wang, W. L. Reduced CO2 uptake and growing nutrient sequestration from slowing overturning circulation. *Nat. Clim. Chang.* **13**, 83–90 (2022).

80. Long, M. C. *et al.* Simulations With the Marine Biogeochemistry Library (MARBL). *J Adv Model Earth Syst* **13**, (2021).

81. Abraham, E. R. *et al.* Importance of stirring in the developmentofan iron-fertilized phytoplankton bloom. *Nature* **407**, 727–730 (2000).

82. Maldonado, M. T. & Price, N. M. Utilization of iron bound to strong organic ligands by plankton communities in the subarctic Pacific Ocean. *Deep-Sea Research II* **46**, 2447 (1999).

83. McKay, R. M. L. *et al.* Impact of phytoplankton on the biogeochemical cycling of iron in subantarctic waters southeast of New Zealand during FeCycle: PHYTOPLANKTON AND THE BIOGEOCHEMICAL CYCLING OF IRON. *Global Biogeochem. Cycles* **19**, (2005).

84. Sarthou, G. *et al.* The fate of biogenic iron during a phytoplankton bloom induced by natural fertilisation: Impact of copepod grazing. *Deep Sea Res. Part 2 Top. Stud. Oceanogr.* **55**, 734–751 (2008).

85. Tovar-Sanchez, A., Sañudo-Wilhelmy, S. A., Garcia-Vargas, M., Weaver, R. S. & Popels Linda C and Hutchins, D. A. A trace metal clean reagent to remove surface-bound iron from marine phytoplankton. *Mar. Chem.* **82**, 91–99 (2003).

86. Twining, B. S., Nuñez-Milland, D., Vogt, S., Johnson, R. S. & Sedwick, P. N. Variations in Synechococcus cell quotas of phosphorus, sulfur, manganese, iron, nickel, and zinc within mesoscale eddies in the Sargasso Sea. *Limnol. Oceanogr.* **55**, 492–506 (2010).

87. Twining, B. S. *et al.* Metal quotas of plankton in the equatorial Pacific Ocean. *Deep Sea Res. Part 2 Top. Stud. Oceanogr.* **58**, 325–341 (2011).

88. Garcia, H. *et al.* World Ocean Atlas 2018. Vol. 4: Dissolved Inorganic Nutrients (phosphate, nitrate and nitrate+nitrite, silicate). *NOAA Atlas NESDIS 84* 35pp (2019).

89. GEOTRACES Intermediate Data Product Group. The GEOTRACES Intermediate Data Product 2021 (IDP2021). Preprint at (2021).

90. Tagliabue, A. *et al.* A global compilation of dissolved iron measurements: focus on distributions and processes in the Southern Ocean. *Biogeosciences* **9**, 2333–2349 (2012).

91. Sholkovitz, E. R., Sedwick, P. N., Church Thomas M and Baker, A. R. & Powell, C. F. Fractional solubility of aerosol iron: Synthesis of a global-scale data set. *Geochim. Cosmochim. Acta* **89**, 173–189 (2012).

92. Liu, M. *et al.* The underappreciated role of anthropogenic sources in atmospheric soluble iron flux to the Southern Ocean. *NPJ Clim Atmos Sci* **5**, 1–9 (2022).

93. Anderson, R. F. GEOTRACES: Accelerating Research on the Marine Biogeochemical Cycles of Trace Elements and Their Isotopes. *Ann. Rev. Mar. Sci.* **12**, 49–85 (2020).

94. Moore, J. K. *et al.* Sustained climate warming drives declining marine biological productivity. *Science (1979)* **359**, 1139–1143 (2018).

95. DeVries, T., Primeau, F. & Deutsch, C. The sequestration efficiency of the biological pump. *Geophys. Res. Lett.* **39**, (2012).

96. Kwon, E. Y., Primeau, F. & Sarmiento, J. L. The impact of remineralization depth on the air–sea carbon balance. *Nature Geoscience* vol. 2 630–635 Preprint at (2009).

97. Passow, U. & Carlson, C. A. The biological pump in a high CO2 world. *Mar. Ecol. Prog. Ser.* **470**, 249–271 (2012).

98. Sarmento, H., Montoya, J. M., Vázquez-Dom\'\inguez, E., Vaqué, D. & Gasol, J. M. Warming effects on marine microbial food web processes: how far can we go when it comes to predictions? *Philos. Trans. R. Soc. Lond. B Biol. Sci.* **365**, 2137–2149 (2010).

99. Tanioka, T. *et al.* Global patterns and predictors of C:N:P in marine ecosystems. *Commun Earth Environ* **3**, (2022).

100. Wiseman, N. A., Moore, J. K., Twining, B. S. & Hamilton D S and Mahowald, N. M. Acclimation of phytoplankton Fe:C ratios dampens the biogeochemical response to varying atmospheric deposition of soluble iron. *Global Biogeochem. Cycles* (2023).

101. Tanioka, T. *et al.* Global Ocean Particulate Organic Phosphorus, Carbon, Oxygen for Respiration, and Nitrogen (GO-POPCORN). *Sci Data* **9**, 688 (2022).

102. Teng, Y.-C., Primeau, F. W., Moore J Keith and Lomas, M. W. & Martiny, A. C. Global-scale variations of the ratios of carbon to phosphorus in exported marine organic matter. *Nat. Geosci.* **7**, 895 (2014).

103. Takeda, S. Influence of iron availability on nutrient consumption ratio of diatoms in oceanic waters. *Nature* **393**, 774–777 (1998).

104. Mosseri, J., Quéguiner, B., Armand, L. & Cornet-Barthaux, V. Impact of iron on silicon utilization by diatoms in the Southern Ocean: A case study of Si/N cycle decoupling in a naturally iron-enriched area. *Deep Sea Res. Part 2 Top. Stud. Oceanogr.* **55**, 801–819 (2008).

105. Christina, L., Hutchins, D. A., Brzezinski, M. A. & Zhang, Y. Effects of iron and zinc deficiency on elemental composition and silica production by diatoms. *Mar. Ecol. Prog. Ser.* **195**, 71–79 (2000).

106. Westberry, T., Behrenfeld, M. J. & others. Carbon-based primary productivity modeling with vertically resolved photoacclimation. *Global Biogeochem. Cycles* (2008).

107. DeVries, T. & Weber, T. The export and fate of organic matter in the ocean: New constraints from combining satellite and oceanographic tracer observations. *Global Biogeochem. Cycles* **31**, 535–555 (2017).

108. Fu, W., Randerson, J. T. & Moore, J. K. Climate change impacts on net primary production (NPP) and export production (EP) regulated by increasing stratification and phytoplankton community structure in the CMIP5 models. *Biogeosciences* **13**, 5151–5170 (2016).

109. Letscher, R. T. & Moore, J. K. Preferential remineralization of dissolved organic phosphorus and non-Redfield DOM dynamics in the global ocean: Impacts on marine productivity, nitrogen fixation, and carbon export. *Global Biogeochem. Cycles* **29**, 325–340 (2015).

110. Tagliabue, A. *et al.* A global compilation of dissolved iron measurements: focus on distributions and processes in the Southern Ocean. *Biogeosciences* **9**, 2333–2349 (2012).

111. Klausmeier, C. A., Litchman, E., Daufresne, T. & Levin, S. A. Optimal nitrogen-to-phosphorus stoichiometry of phytoplankton. *Nature* **429**, 171–174 (2004).

112. Browning, T. J. *et al.* Nutrient co-limitation at the boundary of an oceanic gyre. *Nature* **551**, 242–246 (2017).

113. Wiseman, N., Moore, J. K., Martiny, A. C. & Letscher, R. Phytoplankton variable stoichiometry modifies key biogeochemical fluxes and the functioning of the biological pump. (2023).

114. Arrigo, K. R. Marine microorganisms and global nutrient cycles. *Nature* **437**, 349–355 (2005).

115. Davidson, E. A. & Howarth, R. W. Nutrients in synergy. *Nature* 1000–1001 (2007) doi:10.1111/j.1461.

116. Wu, J., Sunda, W., Boyle, E. A. & Karl, D. M. Phosphate depletion in the western North Atlantic Ocean. *Science (1979)* **289**, 759–762 (2000).

APPENDIX A: Supplementary Material

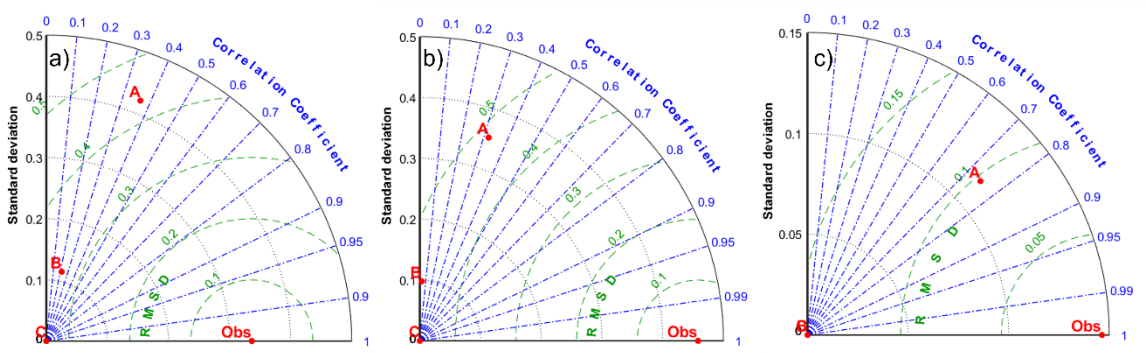

Figure S1.1. Taylor diagram (Taylor, 2001) showing model performance for a) small phytoplankton Fe:C, b) diatom Fe:C, and c) diazotroph Fe:C where model A is the optimized variable model, B is the limited-range variable model, and C and is fixed model with an Fe:C of 5 µmol/mol.

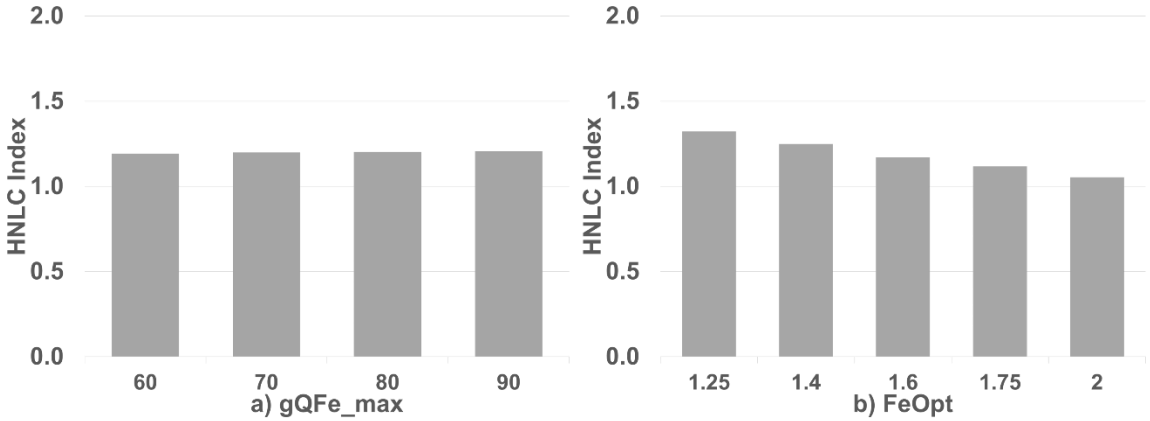

Figure S1.2. HNLC index for tuning exercises where a) gQFe_max varies and FeOpt is held proportionally constant (1.5 nM for 90 µmol/mol, 1.33 nM for 80 µmol/mol, 1.17 nM for 70 µmol/mol, 1.0 nM for 60 µmol/mol) and b) where FeOpt varies and gQFe_max is held constant (90 µmol/mol).

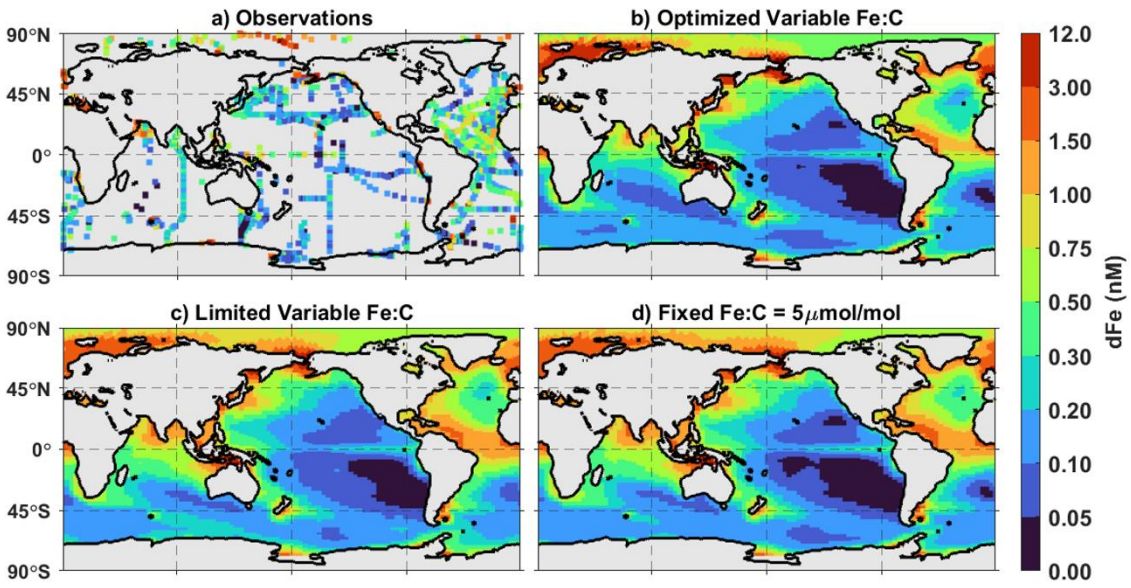

Figure S1.3. Dissolved iron concentrations for the top 100m from a) observations, b) the optimized variable range model, c) the limited variable range model, and d) the tuned fixed model with an iron to carbon of 5 μmol/mol.

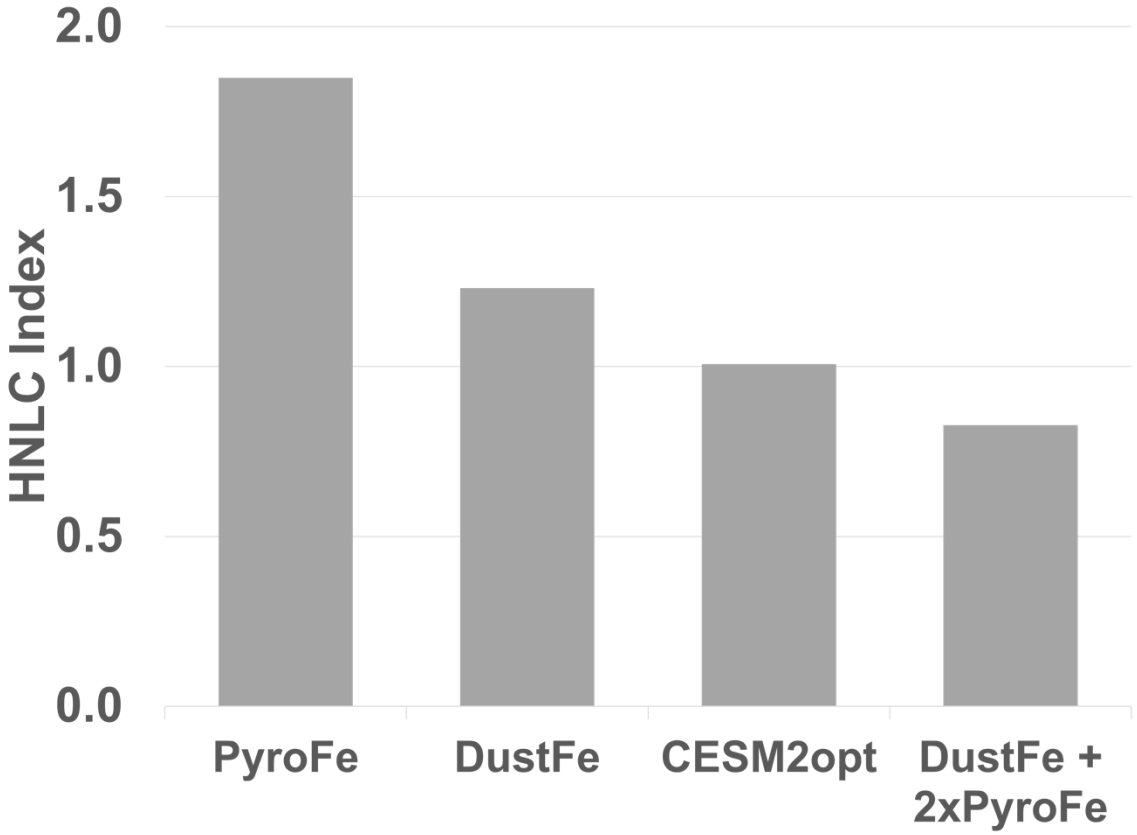

Figure S1.4. HNLC index for four simulations within the Central Pacific HNLC region (between 25°N and 25°S, east of 150°E) under the various iron deposition scenarios for the optimized variable model. Index is defined as the ratio of ocean surface area where nitrate concentrations exceed 0.3 μM in each simulation compared to the WOA18.

Study	Technique	Cell Type	Location	Mean Fe:C
Unpublished	SXRF	aflag	Arctic	50
Unpublished	SXRF	diatom	Arctic	107
(Twining et al., 2021)	SXRF	aflag	Subtropical Pacific	26
(Twining et al., 2021)	SXRF	diatom	Subtropical Pacific	65
(Twining et al., 2021)	SXRF	diatom	Coastal North Pacific	155
(Twining et al., 2021)	SXRF	diatom	Coastal North Pacific	49
(Twining et al., 2021)	SXRF	diatom	North Pacific	38
(Twining et al., 2019)	SXRF	aflag	Indian Ocean	6
(Twining et al., 2015)	SXRF	aflag	North Atlantic	43
(Twining et al., 2015)	SXRF	diatom	North Atlantic	100
(King et al., 2012)	SXRF	aflag	Subtropical Pacific	21
(King et al., 2012)	SXRF	diatom	Subtropical Pacific	21
(Twining et al., 2011)	SXRF	aflag	Equatorial Pacific	17
(Twining et al., 2011)	SXRF	diatom	Equatorial Pacific	14
(Twining et al., 2010)	SXRF		North Atlantic	13
(Twining et al., 2004)	SXRF	aflag	Southern Ocean	11
(Twining et al., 2004)	SXRF	diatom	Southern Ocean	5
(Tovar-Sanchez et al., 2003)	GFAAS			10
(Sañudo-Wilhelmy et al., 2001)	GFAAS	diaz	North Atlantic	35
(Hopkinson et al., 2013)	Radioisotope Uptake		Southern Ocean	10
(Sarthou et al., 2008)	Radioisotope Uptake	aflag	Southern Ocean	8
(Sarthou et al., 2008)	Radioisotope Uptake	diatom	Southern Ocean	4
(McKay et al., 2005)	Radioisotope Uptake	aflag	Southern Ocean	19
(McKay et al., 2005)	Radioisotope Uptake	diatom		6
(Abraham et al., 2000)	Radioisotope Uptake		Southern Ocean	3
(Maldonado & Price, 1999)	Radioisotope Uptake		Central North Pacific	4
(Schmidt & Hutchins, 1999)	Radioisotope Uptake		Central North Pacific	9

Table S1.1. Field observations of Fe:C summarized by study location and cell type. For bulk measurements cell type is left blank.

Study	NO_3 r_s	NO_3 RMSE	PO_4 r_s	PO_4 RMSE	dFe r_s	dFe RMSE
Fixed 3	0.900	2.55	0.920	0.190	0.442	1.290
Fixed 5	0.900	2.33	0.937	0.157	0.449	1.288
Fixed 7	0.867	2.41	0.930	0.178	0.454	1.286
Fixed 10	0.778	3.26	0.919	0.198	0.468	1.282
Limited variable range	0.916	2.41	0.924	0.188	0.445	1.288
Optimized variable range	0.909	2.29	0.928	0.181	0.490	1.265

Table S1.2. Spearman's r_s and root mean squared error (RMSE) for model surface (0-5m) nitrate and phosphate compared to World Ocean Atlas 2018 for the fixed Fe:C iterations, previous limited variable range (Moore 2004) and the expanded variable range models, Spearman's correlation r_s and root mean squared error for model iron (all depths) is compared to observations from GEOTRACES and supplemental observations (full dataset is available in the data repository).

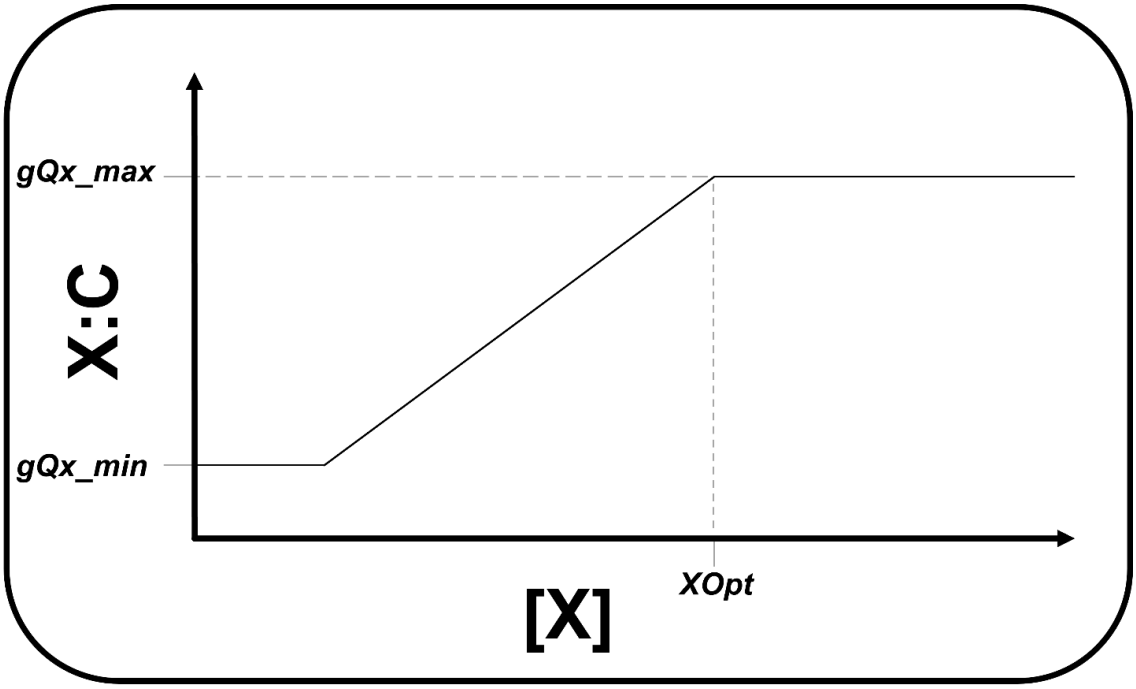

Figure S2.1. Phytoplankton nutrient to carbon (X:C) ratio for new growth as a function of dissolved ambient nutrient concentration [X]. XOpt determines the dissolved ambient nutrient concentration at which phytoplankton X:C reaches it maximum value (gQx_max). X:C decreases linearly with decreasing dissolved nutrient concentration between the prescribed, group-specific maximum (gQx_max) and minimum (gQx_min) quotas. X here applies for nitrogen, phosphorus, iron, and silica.

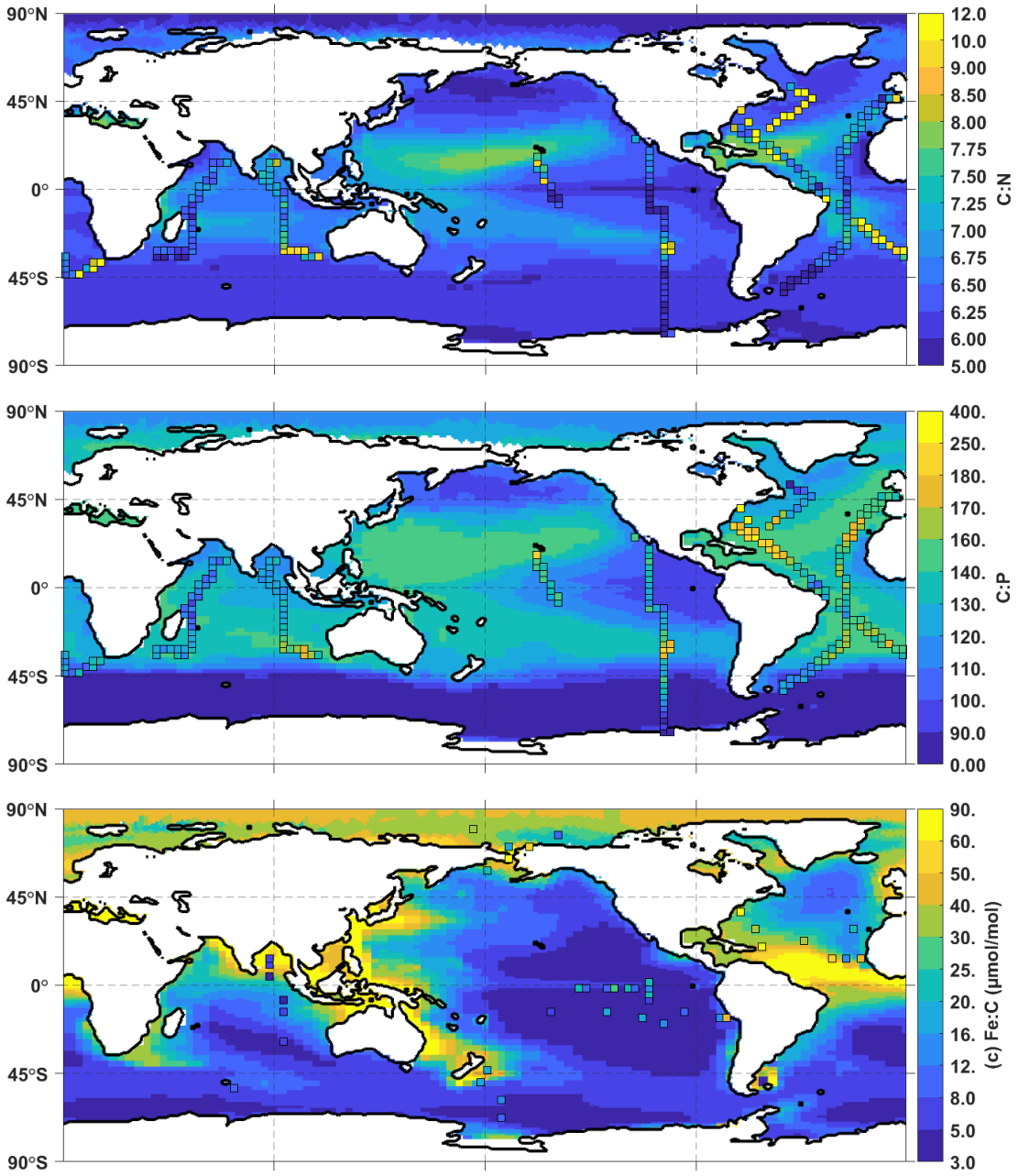

Figure S2.2. Export particulate organic carbon to phosphorus and nitrogen (C:P, C:N) ratio for VarAll case overlaid with surface (5m) particulate C:P and C:N from the GO-POPCORNv2 database[101]. GO-POPCORNv2 data is averaged into 3 degree x 3 degree bins for visualization purposes. Model small phytoplankton iron to carbon (Fe:C) ratio for VarAll case overlaid with observations of autotrophic flagellate cellular Fe:C compiled from Wiseman et al., 2023[100].

Table S2.1. Model parameters for phytoplankton nutrient quotas

	Small Phytoplankton	Diatoms	Diazotrophs
NOpt, gQn_min, gQn_max	0.4, 0.111, 0.167	0.4, 0.111, 0.167	0.4, 0.143, 0.167
POpt, gQp_min[1], gQp_max	1.0, 0.004, 0.013	1.0, 0.008, 0.011	1.0, 0.004, 0.008
FeOpt, gQfe_min, gQfe_max	1.3, 3.0, 90.0	1.3, 3.0, 90.0	1.6, 4.5, 135.0
SiOpt, gQsi_min, gQsi_max	N/A		N/A

[1]P:C minimum quotas can be reduced to a smaller value due to the N:P scaling

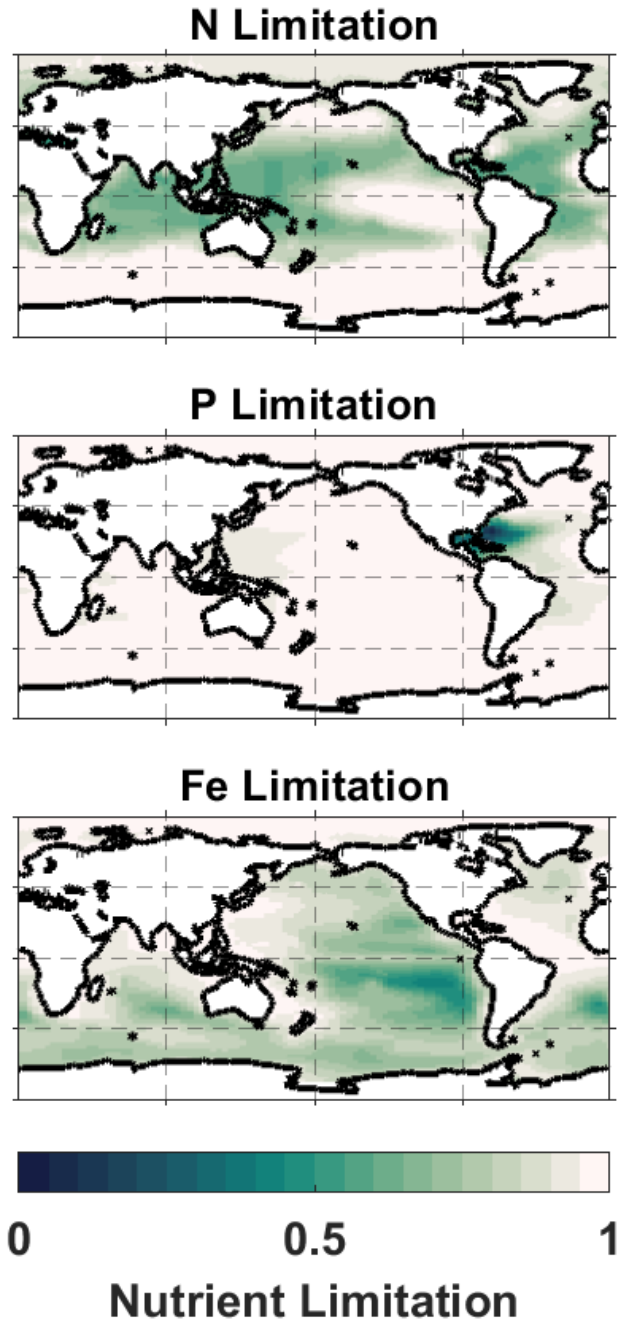

Figure S3.1. Degree of nutrient stress for small phytoplankton in the VarAll simulation. Darker colors indicate greater reduction in the relative growth rate due to nutrient stress.

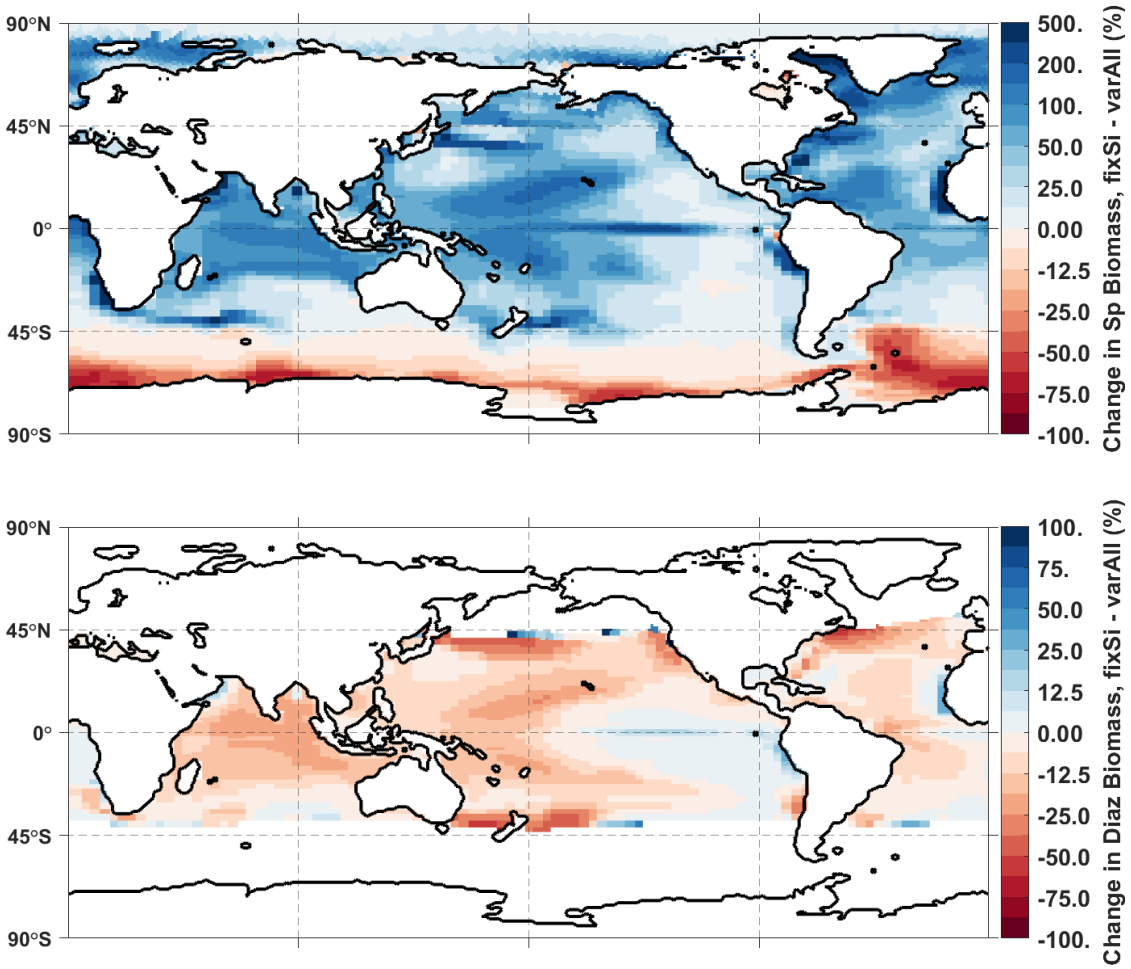

Figure S3.2. Change in biomass for (**a**) small phytoplankton and (**b**) diazotrophs when Si quotas are fixed.